

Degenerate quantum erasure decoding

Kao-Yueh Kuo^{1,*} and Yingkai Ouyang^{1,†}

¹*School of Mathematical and Physical Sciences, University of Sheffield, Sheffield, S3 7RH, United Kingdom*

Erasures are the primary type of errors in physical systems dominated by leakage errors. While quantum error correction (QEC) using stabilizer codes can combat erasure errors, it remains unknown which constructions achieve capacity performance. If such codes exist, decoders with linear runtime in the code length are also desired. In this paper, we present erasure capacity-achieving quantum codes under maximum-likelihood decoding (MLD), though MLD requires cubic runtime in the code length. For QEC, using an accurate decoder with the shortest possible runtime will minimize the degradation of quantum information while awaiting the decoder's decision. To address this, we propose belief propagation (BP) decoders that run in linear time and exploit error degeneracy in stabilizer codes, achieving capacity or near-capacity performance for a broad class of codes, including bicycle codes, product codes, and topological codes. We furthermore explore the potential of our BP decoders to handle mixed erasure and depolarizing errors, and also local deletion errors via concatenation with permutation invariant codes.

I. INTRODUCTION

Erasure conversion is a recent technique that converts leakage errors into erasures. In systems dominated by leakage errors, such as ultracold Rydberg atoms [1–5], superconducting circuits [6–8], trapped ions [9], or photonic systems [10], erasure conversion ensures that the majority of errors are erasures. In the context of quantum error correction (QEC), the promised structure of errors affords potentially better error thresholds and decoding efficiency compared to unstructured errors. We aim to explore optimal QEC performance in erasure-dominated systems.

The rate of a QEC code is the ratio of the number of encoded qubits k to the number of physical qubits n . The quantum erasure channel capacity, $C(p) = 1 - 2p$ [11, 12], represents the maximum rate (k/n) for which a decoder can almost surely correct typical erasures, where p is the independent erasure probability per qubit. This capacity quantifies the highest rate of reliable quantum information transmission over a noisy erasure channel. A central question in quantum information theory is: how closely can practical QEC codes approach $C(p)$ with low-complexity decoders?

This question is particularly pertinent for quantum stabilizer codes with code parameters $[[n, k]]$ and low-weight commutative Pauli operators¹, known as quantum low-density parity-check (QLDPC) codes. Two outstanding open problems in this area are: (1) identifying stabilizer code constructions that achieve capacity $r = 1 - 2p$ for arbitrary rates $r = k/n$, and (2) developing decoders that enable these constructions to achieve near-capacity performance with linear runtime complexity. This paper solves both of these problems.

Previously, only two-dimensional (2D) topological codes, such as surface or toric codes, were known to achieve erasure capacity [13, 14] with linear decoding time [15], but their code rate vanishes ($r \rightarrow 0$) as n increases.

A recent breakthrough by IBM significantly reduce qubit overhead ($1 - \frac{k}{n}$) compared to surface codes, using non-zero rate QLDPC codes—specifically bivariate bicycle codes—highlighting their non-vanishing rate and potential for nearly 2D layouts [16]. Bicycle-type codes with hundreds of qubits achieve comparable performance to surface codes with thousands, protecting a similar number of information qubits, offering a 10 times reduction in the number of physical qubits.

A further significant reduction in qubit overhead can be achieved using higher-rate codes, with long code lengths ensuring the correction of a large fraction of errors, which we include in this work. First, we show that the bicycle construction [17] achieves capacity for moderate-to-high rate codes on the quantum erasure channel. Second, for low-rate (but non-zero rate) cases, product constructions with flexible rate, such as lifted-product (LP) codes [18], also achieve erasure capacity. Third, to facilitate practical applications, we provide linear-time decoders universal for these codes, also supporting vanishing-rate 2D topological codes.

For erasures, the task of decoding (inferring the error) reduces to solving a system of linear equations (cf. (3)–(7)). The optimal decoder is the maximum-likelihood decoder (MLD), which is often implemented using a Gaussian decoder. This approach employs Gaussian elimination with a complexity of $O(n^3)$, or $O(n^{2.373})$ [19, 20].

In classical erasure error-correction, a binary bit-flipping belief propagation (Flip-BP₂) decoder is preferred over MLD for classical LDPC codes due to its linear runtime $O(n)$ and near-capacity performance [21–27]. The success of BP is evident in 5G networks [28, 29]. However, naively applying Flip-BP₂ to QLDPC codes is problematic due to inevitable small stopping sets in the quantum case (see Appendix C). Small stopping sets obstruct BP convergence [23–27, 30, 31] and are avoided in the classical code design [24–27].

In the quantum case, various techniques have been proposed for decoding QLDPC codes under erasures. First, the peeling decoder was proposed to decode 2D topological codes, including peeling on toric or surface codes (in linear time) [15] or extended peeling on color codes (with additional complexity) [32–34]. (The peeling decoder includes

* k.kuo@sheffield.ac.uk

† y.ouyang@sheffield.ac.uk

¹ The weight of a Pauli operator is the number of its non-identity components. The weight of a binary vector is its Hamming weight.

a spanning-tree step [35], and a peeling step, resembling a Flip-BP₂ in [22] as pointed in [36].) Second, for product codes, the pruned peeling, improved over the peeling decoder, and a Vertical-Horizontal (VH) post-processing are proposed [36]. The “pruned peeling + VH” has complexity $O(n^2)$, or $O(n^{1.5})$ for a probabilistic version. Third, modifications of minimum-weight perfect matching (MWPM) have good erasure decoding accuracy for 2D codes [9, 37], though without linear time [38]. Recently, BP with guided decimation is explored [39], and cluster decomposition is introduced [40] by extending the VH technique, aiming to balance accuracy and complexity between MLD and VH, where both [39, 40] focusing on product codes.

In this paper, we study a broad class of QLDPC codes, including CSS ([41, 42]) and non-CSS (e.g., XZZX) 2D topological codes [43–46], [47–49], bicycle codes [17], hypergraph-product (HP) codes [50], generalized HP (GHP) codes [51], and LP codes [18]. General QLDPC codes admit low-complexity quantum circuits and offer the benefits of (1) enabling error-corrected quantum computation with constant encoding rates [52, 53] and (2) enhancing quantum network communication rates [54].

In our approach, we define *erasure bounded-distance decoding* (eBDD) (Def. 3) as a metric for evaluating decoding accuracy. We estimate the error threshold p_{th} of a code family by checking whether a constant correction radius t/n exists as n increases, where t is the expected number of corrected erasures. If so, we set $p_{\text{th}} = t/n$. For clarity, we may denote $p_{\text{th}}^{(\text{BP})}$ for BP and $p_{\text{th}}^{(\text{MLD})}$ for MLD if they differ.

Quantum decoding relies on exploiting degeneracy, enabling a decoder to converge to any (degenerate) error equivalent to the occurred error up to a stabilizer, resulting in remarkable accuracy [55–57]. Our constructed codes achieve capacity performance with $r = 1 - 2p_{\text{th}}^{(\text{MLD})}$ using the Gaussian decoder (MLD), which always finds a solution likely to be a degenerate error, at the cost of $O(n^3)$ complexity. To achieve linear runtime $O(n)$, we first propose a gradient-descent Flip-BP₂ (GD Flip-BP₂) to address stopping sets via a simple GD scheme (which is supported by the symmetry of degenerate errors; see [55] or Appendix D). Next, we introduce a soft binary BP with memory effects (MBP₂), its adaptive version (AMBP₂), and their quaternary counterparts (A)MBP₄. A soft BP decoder mimics a soft GD optimization, providing strong convergence to degenerate solutions. For our constructed codes, we achieve near-capacity performance with $r = 1 - 2.5p_{\text{th}}^{(\text{BP})}$ using (A)MBP or GD Flip-BP₂ for non-zero rate codes, with AMBP providing very strong accuracy at low error rates. In addition, AMBP₄ achieves the optimal threshold of 0.5 for vanishing-rate 2D topological codes.

The success of (A)MBP stems from multiple factors. First, we apply message softization (15) to have non-extreme, and non-zero BP message values, enabling updates within stopping sets. Second, we link BP to gradient descent to determine a proper update step-size and, when necessary, adjust the prior error distribution to ensure sufficient update gradients, further mitigating harmful stopping sets (Sec. IV A). Third, we extend binary decoders to quater-

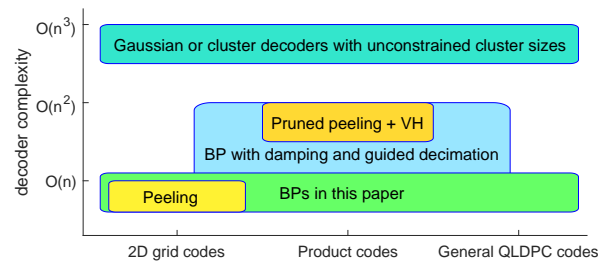


FIG. 1: Comparison of decoders. The vertical axis indicates decoder complexity, while the horizontal axis shows code types with increasing connectivity from left to right. BPs in this paper perform accurately across various code types, similar to the Gaussian decoder, with a slight threshold gap but with linear complexity. The achieved thresholds are shown in Fig. 2.

nary ones, leveraging correlations between the X -portion and Z -portion of a QLDPC check matrix to prevent BP from being halted by stopping sets in one portion. Moreover, inspired by Hopfield nets [58–60], (A)MBP uses fixed inhibition (see Appendix E 2), adding memory effects to BP to improve convergence. Additionally, we employ a group random schedule for message updates to improve convergence, similar to a serial schedule [61], while processing multiple messages in parallel (see Appendix H). Finally, we propose a strategy to make AMBP as efficient as MBP to facilitate practical applications.

We also explore the potential of our decoders to manage deletions of untracked particle losses (with the assistance of permutation-invariant (PI) codes [62, 63]) or mixed erasure and depolarizing errors.

II. RESULTS

Figure 1 compares the decoding complexity of various decoders. BPs developed in this paper have accuracy comparable to the Gaussian decoder (MLD), but with linear complexity. The thresholds achieved by BP and MLD are analysed and compared with the channel capacity in Fig. 2. Physical fidelity decays exponentially over time (characterized by the decoherence time [3, 65]). We plot the erasure error rate p on a log scale to depict the exponential effort to maintain coherence. In Fig. 2, except for the 2D topological codes, each code family is represented by two data points, indicating the thresholds achieved by BP and MLD. There is a small gap between the accuracy of BP (linear-time decoder) and MLD (non-linear time decoder). The each code family has nearly fixed row and column weights to ensure linear BP complexity (see Appendix G 2).

In Fig. 2, we also plot rate upper bounds estimated by [12, Theorem 3.8], which depend on stabilizer weight w . While not necessarily tight, these bounds align with our findings in that higher code rates require higher w .

To obtain a precise estimate of the rate currently achieved via BP at erasure probability p , we replot Fig. 2 on a linear scale in Appendix G 6 (Fig. 22). By interpolation, the rate

TABLE I: Comparison of linear-time and MLD decoders for quantum erasure errors on data qubits.

decoder	type	optimized complexity	worst case complexity	tested codes	comment
Peeling [15]	spanning-tree (MLD for 2D codes)	$O(n)$ (toric/surface)	$O(nT_{\max})$	2D gird (toric/surface) [15]; color codes need additional complexity [32–34]	spanning-tree step is linear-time [35]; peeling step is iterative, but guaranteed to finish within $T_{\max} = O(1)$ iterations for toric/surface codes.
Pruned peeling + VH [36]	spanning tree + local GE	$O(n^{1.5})$ (if use [64])	$O(n^2)$	HP	Peeling needs VH to decode HP codes but underperforms AMBP (Fig. 17)
BP with damping and guided decimation [39]	soft BP + guided decimation	$O(n)$ (reduced accuracy)	$O(n^2T_{\max})$	HP and GHP	outperform peeling+VH, although not as accurate as AMBP (Fig. 18)
Peeling + cluster decomposition [40]	spanning tree + tuneable GE	$O(n)$ (reduced accuracy)	$O(n^3)$ (MLD)	HP and GHP	flexible accuracy/complexity tradeoff; can beat BPs (Fig. 18) but need complexity $O(n^3)$
GD Flip-BP ₂ (this paper, Algorithms 1)	bit-flipping BP	$O(n \log \log n)$	$O(nT_{\max})$	LP (Fig. 8), bicycle (Fig. 6), HP and GHP (Figs. 11, 17, and 18)	performs well on bicycle and rate 0.118 LP codes; extremely low complexity
(A)MBP _q ($q = 2$ or 4) (this paper, Algorithms 2–4)	soft BP	$O(n \log \log n)$	$O(nT_{\max})$	LP (Figs. 7 and 20), bicycle (Fig. 19), toric and XZZX (Figs. 9 and 21), HP and GHP (Figs. 11, 17, and 18)	accurate and universal for QLDPC codes; also decode mixed errors with high accuracy (Fig. 5)
Gaussian elimination (GE) (see (6)–(7))	MLD	$O(n^{2.373})$ (see [19, 20])	$O(n^3)$	we provide the accuracy achieved by Gaussian decoder for all tested codes	MLD is difficult to simulate at low error rates, but eBDD provides good curve extrapolation

Upper portion: decoders in the literature; Lower portion: our decoders and GE. GHP codes are considered as special LP codes [18, 39, 40]. We construct flexible-rate and flexible-length LP codes from random quasi-cyclic matrices and bicycle codes with random generator vectors. High-rate bicycle codes ($r = 3/4$) are particularly suitable to work with PI codes for local deletion errors (cf. Fig. 4). Bicycle codes are generalized for fault-tolerant error correction on IBM hardware implementations, emphasizing their non-zero code rate and potential for nearly 2D layouts [16].

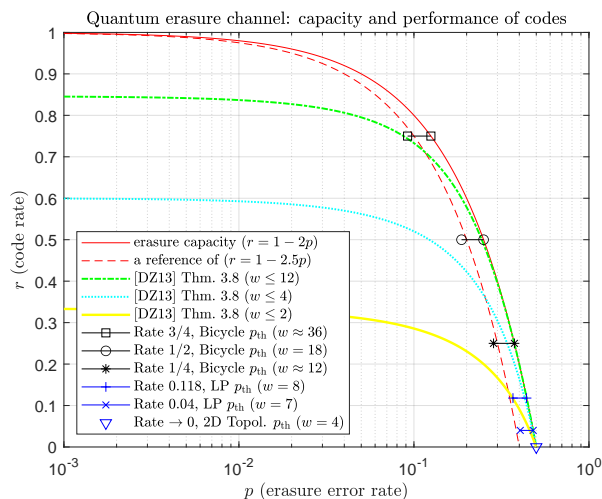


FIG. 2: Quantum erasure capacity and thresholds of codes. For 2D topological codes, BP and MLD share a threshold of $p_{\text{th}} = 0.5$. For other codes, a small accuracy gap is indicated by two points: $p_{\text{th}}^{(\text{BP})}$ (left) and $p_{\text{th}}^{(\text{MLD})}$ (right). The constructed codes achieve capacity with MLD, $r = 1 - 2p_{\text{th}}^{(\text{MLD})}$, and near-capacity with BP, $r = 1 - 2.5p_{\text{th}}^{(\text{BP})}$.^a Higher-rate codes require larger stabilizer weight w , consistent with the results in [12] ([DZ13]).

^a We summarize our decoders and tabulate their accuracy figures in Table I. For bicycle codes, BP thresholds are achieved using GD Flip-BP₂ or (A)MBP_q. For LP codes, BP thresholds are achieved using AMBP_q, and GD Flip-BP₂ shows similar accuracy for rate 0.118 LP codes. For 2D topological codes, a threshold of 0.5 is achieved using AMBP₄.

achieved by BP is $r = 1 - 2.5p - 2p^2 + 6p^3$.

In Table I, we compare our results with other linear-time or MLD decoders in the literature [15, 36, 39, 40].

A. Quantum erasure channel

Erasures occur when certain qubits are lost, with a detector identifying their locations. A lost qubit is represented by an “erasure state” $|2\rangle$, orthogonal to the computational basis states $|0\rangle$ and $|1\rangle$. Thus, we consider [11, 12]:

Definition 1. A quantum erasure channel independently erases each qubit ρ_1 with probability $p \leq 0.5$, leaving it unchanged otherwise, resulting in the following error process:

$$\rho_1 \mapsto (1-p)\rho_1 + p|2\rangle\langle 2|, \quad (1)$$

with the location of the erased qubit known.

Assume that an $[[n, k]]$ stabilizer code is used. For decoding, we insert an ancilla qubit at each lost qubit’s location, creating a noisy codeword state of length n for stabilizer measurements. After measurements, each ancilla qubit collapses randomly, encountering Pauli I, X, Y , or Z with equal probability $1/4$. Thus, an erased qubit (with its location known) encounters the following error before decoding:

$$\rho_1 \mapsto (1-p)\rho_1 + p\frac{I}{2}, \quad (2)$$

where $\frac{I}{2} = \sum_{W \in \{I, X, Y, Z\}} \frac{1}{4} W \rho_1 W^\dagger$. The error process (2) is similar to the depolarizing channel, but with a key distinction: we know which qubits are completely depolarized.

Let $\mathfrak{r} \subseteq \{1, 2, \dots, n\}$ be the set of *erased coordinates*. If $j \in \mathfrak{r}$, then qubit j is erased. The complement, $\bar{\mathfrak{r}} = \{1, 2, \dots, n\} \setminus \mathfrak{r}$, contains the *non-erased coordinates*.

Let $E = E_1 \otimes \dots \otimes E_n$ be the n -fold Pauli error (up to global phase) after measurements, where $E_j = I, X, Y$, or Z with equal probability $\frac{1}{4}$ if $j \in \mathfrak{r}$, and $E_j = I$ if $j \in \bar{\mathfrak{r}}$.

A stabilizer decoder infers E from \mathfrak{r} and the *syndrome* of E obtained through measurements, as detailed below.

B. Erasure decoding problem in stabilizer codes

We refer to [66, 67] for stabilizer codes. For stabilizer decoding problem, we represent the measured stabilizers $H^{(1)}, \dots, H^{(n-k)}$ as a (quaternary) Pauli check matrix

$$H = \begin{bmatrix} H^{(1)} \\ \vdots \\ H^{(n-k)} \end{bmatrix} \in \{I, X, Y, Z\}^{(n-k) \times n}. \quad (3)$$

To have a linear decoding problem, we map I, X, Y, Z to $(0|0), (1|0), (1|1), (0|1)$, respectively. Conventionally, this defines a map $\varphi : \{I, X, Y, Z\}^n \rightarrow \{0, 1\}^{2n}$, and we have a $(n-k) \times 2n$ binary check matrix

$$H = \begin{bmatrix} \varphi(H^{(1)}) \\ \vdots \\ \varphi(H^{(n-k)}) \end{bmatrix} = \begin{bmatrix} H_1 \\ \vdots \\ H_{n-k} \end{bmatrix} = \begin{bmatrix} H_{1,1} & \dots & H_{1,2n} \\ \vdots & \ddots & \vdots \\ H_{n-k,1} & \dots & H_{n-k,2n} \end{bmatrix} \quad (4)$$

$$= [H^X | H^Z] = \begin{bmatrix} H_{1,1}^X & \dots & H_{1,n}^X & | & H_{1,1}^Z & \dots & H_{1,n}^Z \\ \vdots & \ddots & \vdots & | & \vdots & \ddots & \vdots \\ H_{n-k,1}^X & \dots & H_{n-k,n}^X & | & H_{n-k,1}^Z & \dots & H_{n-k,n}^Z \end{bmatrix}. \quad (5)$$

Consider the operation under mod 2 for the binary field $\mathbb{F}_2 = \{0, 1\}$. For two binary matrices A and B of $2n$ columns, define a bilinear form (called symplectic inner product)

$$\langle A, B \rangle = A \Lambda B^T,$$

where $\Lambda = \begin{bmatrix} 0_n & 1_n \\ 1_n & 0_n \end{bmatrix}$ and $(\cdot)^T$ is the matrix transpose. Two operators $E, F \in \{I, X, Y, Z\}^n$ commute if the corresponding \mathbf{E}, \mathbf{F} satisfy $\langle \mathbf{E}, \mathbf{F} \rangle = 0$, and anticommute if $\langle \mathbf{E}, \mathbf{F} \rangle = 1$. We denote zero and identity matrices by $\mathbf{0}$ and $\mathbf{1}$, respectively, using the subscript n to specify dimension $n \times n$. Notice that $\langle \mathbf{H}, \mathbf{H} \rangle = \mathbf{0}$. The row-space of \mathbf{H} is a linear code $C = \text{Row}(\mathbf{H}) \subset \mathbb{F}_2^{2n}$, which is symplectic self-orthogonal. That is, $C \subseteq C^\perp$, where C^\perp is the symplectic dual of C in \mathbb{F}_2^{2n} .

For any stabilizer codes, we have this **degeneracy**: for an error $\mathbf{E} \in \{0, 1\}^{2n}$, its logical coset is $\mathbf{E} + C$; any errors $\tilde{\mathbf{E}} \in \mathbf{E} + C$ are degenerate errors of \mathbf{E} with an equivalent effect on the code space. Degenerate errors share the same syndrome $\mathbf{s} = \langle \mathbf{E}, \mathbf{H} \rangle = \langle \tilde{\mathbf{E}}, \mathbf{H} \rangle$, but syndrome matched errors form a larger error set called error coset $(\mathbf{E} + C^\perp)$ of syndrome \mathbf{s} .

Definition 2. (Quantum erasure decoding problem) Given a binary matrix $\mathbf{H} \in \{0, 1\}^{m \times 2n}$, $m \geq n-k$, erasure information $\mathfrak{r} \subseteq \{1, 2, \dots, n\}$, and a syndrome $\mathbf{s} \in \{0, 1\}^m$, where $\mathbf{s} = \langle \mathbf{E}, \mathbf{H} \rangle$ for some $\mathbf{E} \in \{0, 1\}^{2n}$ drawn from the erasure channel, a decoder is asked to find an $\hat{\mathbf{E}} \in \{0, 1\}^{2n}$ such that $\hat{\mathbf{E}} \in \mathbf{E} + C$ with probability as high as possible.

Given \mathfrak{r} and \mathbf{s} , an erasure- and syndrome-matched solution (feasible solution) satisfies a system of linear equations:

$$\begin{cases} (\mathbf{H} \Lambda) \mathbf{E}^T = [\mathbf{H}^Z | \mathbf{H}^X] (\mathbf{E}^X | \mathbf{E}^Z)^T = \mathbf{s}^T, \\ (\mathbf{E}_j^X | \mathbf{E}_j^Z) = (0|0) \quad \forall j \in \bar{\mathfrak{r}}. \end{cases} \quad (6)$$

This can be simplified by solving

$$[\mathbf{H}_{\mathfrak{r}}^Z | \mathbf{H}_{\mathfrak{r}}^X] (\mathbf{E}_{\mathfrak{r}}^X | \mathbf{E}_{\mathfrak{r}}^Z)^T = \mathbf{s}^T, \quad (7)$$

where $A_{\mathfrak{r}}$ denotes the submatrix of a matrix A restricted to the columns specified by \mathfrak{r} . The cardinality $|\mathfrak{r}| \approx np \propto n$. A solution to (6) or (7) can be obtained by Gaussian elimination with complexity $O(n^3)$. Since the syndrome is produced from the error, there always exists at least one solution. The uniqueness of the solution depends on $|\mathfrak{r}|$ and the code distance d (discussed in detail in Appendix B). An $[[n, k]]$ code with distance d is called an $[[n, k, d]]$ code.

Paralleling [15, Lemma 1], we present the following lemma and theorem, proved by group theory and probability theory in Appendix A.

Lemma 1. If two distinct logical cosets both contain feasible solutions, then the number of feasible solutions in both cosets is equal, and they both are maximum likelihood logical cosets.

Theorem 2. For a stabilizer code with a check matrix $\mathbf{H} \in \{0, 1\}^{m \times 2n}$, if erasures $\mathfrak{r} \subseteq \{1, 2, \dots, n\}$ and syndrome $\mathbf{s} \in \{0, 1\}^m$ are given for decoding, then any feasible solution to (6) is an optimal solution for the decoding problem in Def. 2. A decoder always outputting a feasible solution is an MLD.

Obtaining a feasible solution is the best a decoder can do for erasure decoding, although it does not always guarantee successful decoding, especially when $|\mathfrak{r}|$ is large.

Example 1. Consider a $[[4, 1]]$ code with this check matrix

$$\mathbf{H} = [\mathbf{H}^X | \mathbf{H}^Z] = \begin{bmatrix} 1 & 0 & 0 & 0 & | & 0 & 0 & 1 & 0 \\ 0 & 1 & 0 & 1 & | & 0 & 1 & 0 & 1 \\ 0 & 0 & 1 & 1 & | & 1 & 0 & 0 & 1 \end{bmatrix}, \quad (8)$$

or equivalently, its Pauli check matrix

$$\mathbf{H} = \begin{bmatrix} X & I & Z & I \\ I & Y & I & Y \\ Z & I & X & Y \end{bmatrix}. \quad (9)$$

There are $2^{2k} = 4$ logical cosets for a given syndrome \mathbf{s} . When $\mathbf{s} = (010)$, the corresponding 4 logical cosets, in Paulis, are:

$$\begin{bmatrix} I & Z & I & I & \leftarrow \\ X & Z & Z & I \\ I & X & I & Y & \leftarrow \\ X & X & Z & Y \\ Z & Z & X & Y \\ Y & Z & Y & Y \\ Z & X & X & I \\ Y & X & Y & I \end{bmatrix}, \quad \begin{bmatrix} I & I & Z & X \\ X & I & I & X \\ I & Y & Z & Z \\ X & Y & I & Z \\ Z & I & Y & Z \\ Y & I & X & Z \\ Z & Y & Y & X \\ Y & Y & X & X \end{bmatrix}, \quad \begin{bmatrix} I & I & Z & Z \\ X & I & I & Z \\ I & Y & Z & X \\ X & Y & I & X \\ Z & I & Y & X \\ Y & I & X & X \\ Z & Y & Y & Z \\ Y & Y & X & Z \end{bmatrix}, \quad \begin{bmatrix} I & Z & I & Y & \leftarrow \\ X & Z & Z & Y \\ I & X & I & I & \leftarrow \\ X & X & Z & I \\ Z & Z & X & I \\ Y & Z & Y & I \\ Z & X & X & Y \\ Y & X & Y & Y \end{bmatrix},$$

where left arrows indicate the errors to be discussed.

When only the second qubit is erased, we easily identify a unique solution $I Z I I$. MLD always succeeds in this error case.

When the 2nd and 4th qubits are erased, i.e., $\mathfrak{r} = \{2, 4\}$, we have $E_j = I$ for $j \in \bar{\mathfrak{r}} = \{1, 3\}$. As indicated by the left arrows above, the occurred error is a Pauli operator in either

$$\begin{bmatrix} I & Z & I & I \\ I & X & I & Y \end{bmatrix} \quad \text{or} \quad \begin{bmatrix} I & Z & I & Y \\ I & X & I & I \end{bmatrix}. \quad (10)$$

An MLD will output a solution in one of the cosets, but the actual error may lie in the other coset, leading to a logical error rate of $1/2$ in this error case.

We illustrate the error cases in Appendix A (Fig. 12), which helps to understand the coset structure.

A good code can resolve many erasures with $|\mathfrak{r}| = np$ at large p , and we aim to resolve them in linear time.

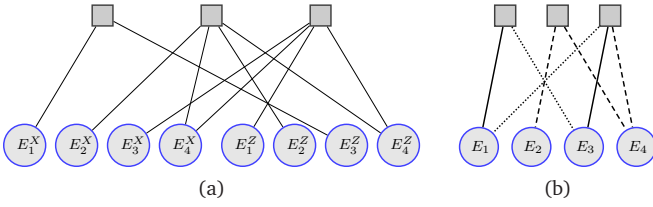


FIG. 3: (a) Tanner graph induced by the binary matrix \mathbf{H} in (8). (b) Tanner graph induced by the Pauli matrix \mathbf{H} in (9), with edge types X (solid line), Y (dashed line), and Z (dotted line).

C. Bit-Flipping BP algorithm

Given (6), BP can approximate the solution with high accuracy, by running a message passing on the Tanner graph induced by the code's check matrix. For classical BP, see [68–72]. For quantum decoding, we can perform binary decoding based on a binary check matrix $\mathbf{H} \in \{0, 1\}^{m \times 2n}$, or a quaternary decoding based on a Pauli check matrix $\mathbf{H} \in \{I, X, Y, Z\}^{m \times n}$. For example, matrices in (8) and (9) induce the two Tanner graphs shown in Fig. 3.

For a Tanner graph, let $\mathcal{N}(i)$ be the set of neighbouring variable node indices of check node i . Let $\mathcal{M}(j)$ be the set of neighbouring check node indices of variable node j . For example, for a Tanner graph induced by an $\mathbf{H} \in \{0, 1\}^{m \times 2n}$,

$$\mathcal{N}(i) = \{j \in \{1, 2, \dots, 2n\} : \mathbf{H}_{ij} = 1\},$$

$$\mathcal{M}(j) = \{i \in \{1, 2, \dots, m\} : \mathbf{H}_{ij} = 1\}.$$

For BP erasure decoding, important code properties include *stopping sets* and *girth*. For details, see Appendix C. However, due to the degeneracy of stabilizer codes, the solutions are generally not unique. Specifically, the number of feasible solutions in a logical coset (Lemma 1) increases with the number of erasures (cf. Example 1). When decoding a code, we aim for the decoder to combat an erasure rate p as high as possible, which leads to many erasures and, consequently, many feasible solutions in the logical coset where the actual error is located. In particular, we observe strong symmetry of degenerate errors (see [55] or more details in Appendix D). This motivates us to use heuristics to converge to any feasible solution. Thus, we propose a bit-flipping algorithm with a gradient descent (GD) step, referred to as GD Flip-BP₂, as outlined in Algorithm 1. (This algorithm behaves more like a greedy approach to minimize a discrete function (11), but can be linked to GD optimization for a differentiable function (18).)

We explain Algorithm 1. The binary check matrix has $2n$ columns. Given $\mathfrak{r} \subseteq \{1, 2, \dots, n\}$, we have

$$\mathfrak{r}_2 = \mathfrak{r} \cup (\mathfrak{r} + n),$$

where $\mathfrak{r} + n = \{j + n : j \in \mathfrak{r}\}$. The GD step performs when no updates are performed during an iteration. This step tries to minimize an objective function defined as the sum of the numbers of unresolved bits in each check, expressed as

$$\sum_{i=1}^m |\mathcal{N}(i) \cap \mathfrak{r}_2|. \quad (11)$$

Algorithm 1 : GD Flip-BP₂

Input:

A binary matrix $\mathbf{H} \in \{0, 1\}^{m \times 2n}$, a syndrome $\mathbf{s} \in \{0, 1\}^m$, erased coordinates $\mathfrak{r}_2 \subseteq \{1, 2, \dots, 2n\}$, and an integer $T_{\max} > 0$. ($\mathbf{H} = [\mathbf{B}^Z | \mathbf{B}^X]$ from a binary check matrix $\mathbf{B} = [\mathbf{B}^X | \mathbf{B}^Z]$.)

Initialization.

- Let $\Gamma_j = 0$ if $j \in \mathfrak{r}_2$, and $\Gamma_j = +1$ if $j \in \bar{\mathfrak{r}}_2$.

Iterative Update.

- For $i \in \{1, 2, \dots, m\}$: Compute $\Delta_i = |\mathcal{N}(i) \cap \mathfrak{r}_2|$; Then if $\Delta_i = 1$, let j be the single element in $\mathcal{N}(i) \cap \mathfrak{r}_2$ and set

$$\Gamma_j = (-1)^{s_i} \prod_{j' \in \mathcal{N}(i) \setminus \{j\}} \Gamma_{j'}.$$

- (GD Step) If no Γ_j is updated in the previous sub-step: Find a $j \in \mathfrak{r}_2$ such that the corresponding column in $\mathbf{H}_{\mathfrak{r}_2}$ has a maximum column weight. Set $\Gamma_j = -1$.
- If any Γ_j is updated during this iteration, remove j from \mathfrak{r}_2 .

Judgement.

- If $\mathfrak{r}_2 = \emptyset$: For all $j = 1, \dots, 2n$, if $\Gamma_j = +1$, set $\hat{E}_j = 0$, and if $\Gamma_j = -1$, set $\hat{E}_j = 1$. Generate $\hat{\mathbf{s}} = \langle \hat{\mathbf{E}}, \mathbf{B} \rangle = \hat{\mathbf{E}} \mathbf{H}^T$.
 - if $\hat{\mathbf{s}} = \mathbf{s}$: return “CONVERGE”;
 - else: return “GD_FAIL”.
 - Else: if the maximum number of iterations T_{\max} is reached, halt and return “FAIL”.
 - Repeat from the step of Iterative Update.
-

D. MBP₂ and its adaptive version (AMBP₂)

A soft-valued decoder improves decoding accuracy. A bit could be 0, 1 or erased (denoted by ?). The values 0, ?, 1 are mapped as +1, 0, -1 in GD Flip-BP₂ for computation. Once a decision is made, ? becomes a bit value 0 or 1 and remains fixed, though it may be incorrect. Generally, we consider a soft-valued decoder, where the messages are represented as soft values, allowing them to adjust their signs and magnitudes during iterations, improving decision accuracy.

We describe this decoder generalization. We have the initial probabilities $p_j^{(0)} = \Pr(\mathbf{E}_j = 0)$ and $p_j^{(1)} = \Pr(\mathbf{E}_j = 1)$ for $j = 1, 2, \dots, 2n$, where

$$(p_j^{(0)}, p_j^{(1)}) = (p_{j+n}^{(0)}, p_{j+n}^{(1)}) = \begin{cases} (\frac{1}{2}, \frac{1}{2}) & \text{if } j \in \mathfrak{r}, \\ (1, 0) & \text{if } j \in \bar{\mathfrak{r}}. \end{cases} \quad (14)$$

The initial *log-likelihood ratios* (LLRs) are $\Lambda_j = \ln(p_j^{(0)}/p_j^{(1)})$ for $j = 1, 2, \dots, 2n$. The (hard) values 0, ?, 1 of \mathbf{E}_j map to $+\infty, 0, -\infty$ as Λ_j . We will update these LLRs, and denote the updated LLRs as Γ_j , $j = 1, 2, \dots, 2n$, to estimate $\hat{\mathbf{E}}_j$.

We restrict variable-to-check messages from taking values in $-\infty, 0, \infty$, avoiding representing the three (hard)

Algorithm 2 : MBP₂ (with an optional soft GD step)

Input:

A binary matrix $\mathbf{H} \in \{0, 1\}^{m \times 2n}$, a syndrome $\mathbf{s} \in \{0, 1\}^m$, an integer $T_{\max} > 0$, a real $\alpha > 0$, and initial LLRs $\Lambda_j = \ln(p_j^{(0)}/p_j^{(1)})$ for $j = 1, 2, \dots, 2n$ (cf. (14)). ($\mathbf{H} = [\mathbf{B}^z | \mathbf{B}^x]$ from a binary check matrix $\mathbf{B} = [\mathbf{B}^x | \mathbf{B}^z]$.)
GD parameters: an integer $T_{\text{GD}} > 0$ and a real $|\Lambda_{\text{GD}}| > 0$.

Initialization.

- For $j \in \{1, 2, \dots, 2n\}$ and $i \in \mathcal{M}(j)$: Let $\Gamma_{j \rightarrow i} = \text{soft}(\Lambda_j)$.

Check-Node Computation.

- For $i \in \{1, 2, \dots, m\}$: Let $\Delta_i = (-1)^{s_i} \boxplus_{j \in \mathcal{N}(i)} \Gamma_{j \rightarrow i}$.
- For $i \in \{1, 2, \dots, m\}$ and $j \in \mathcal{N}(i)$: Let $\Delta_{i \rightarrow j} = \Delta_i \boxminus \Gamma_{j \rightarrow i}$.

Variable-Node computation.

- For $j \in \{1, 2, \dots, 2n\}$: Let $\Gamma_j = \Lambda_j + (1/\alpha) \sum_{i \in \mathcal{M}(j)} \Delta_{i \rightarrow j}$.
- For $j \in \{1, 2, \dots, 2n\}$ and $i \in \mathcal{M}(j)$: Compute

$$\begin{aligned} \Gamma_{j \rightarrow i} &= \Gamma_j - \Delta_{i \rightarrow j}, \\ \Gamma_{j \rightarrow i} &= \text{soft}(\Gamma_{j \rightarrow i}). \end{aligned} \quad (12)$$

- (Optional soft GD Step) When the number of iterations is a multiple of T_{GD} : For $j \in \{1, 2, \dots, 2n\}$,

$$\text{if } |\Gamma_j| < |\Lambda_{\text{GD}}|, \text{ then set } \Lambda_j = \text{sign}(\Gamma_j) |\Lambda_{\text{GD}}|. \quad (13)$$

Judgement.

- For all $j = 1, \dots, 2n$, if $\Gamma_j \geq 0$, set $\hat{E}_j = 0$, and if $\Gamma_j < 0$, set $\hat{E}_j = 1$. Generate $\hat{\mathbf{s}} = \langle \hat{\mathbf{E}}, \mathbf{B} \rangle = \hat{\mathbf{E}} \mathbf{H}^T$.
 - if $\hat{\mathbf{s}} = \mathbf{s}$: return “CONVERGE”;
 - else if the maximum number of iterations T_{\max} is reached: halt and return “FAIL”.
 - else: repeat from the Check-Node Computation step.
-

values 0, ?, 1. The function achieves our purpose:

$$\text{soft}(x) = \begin{cases} \text{sign}(x) \text{LLR_MAX}, & \text{if } |x| > \text{LLR_MAX}, \\ \text{sign}(x) \text{LLR_MIN}, & \text{if } |x| < \text{LLR_MIN}, \\ x, & \text{otherwise.} \end{cases} \quad (15)$$

This maintains LLR numerical stability and enables updates even within stopping sets. Suggested values for LLR_MAX and LLR_MIN are provided in Appendix I.

Remark 3. We do not apply the function $\text{soft}(\cdot)$ in (15) to initial LLRs Λ_j . This ensures $\Gamma_j = \Lambda_j = +\infty$ for $j \in \bar{v}_2$, making our BP output always erasure-matched, though convergence (syndrome matching, $\hat{\mathbf{s}} = \mathbf{s}$) is not guaranteed.

We will update LLRs to meet the target syndrome. For two LLRs Γ_1 and Γ_2 , following Gallager [68], we define

$$\Gamma_1 \boxplus \Gamma_2 := \text{sign}(\Gamma_1 \Gamma_2) f^{-1}(f(|\Gamma_1|) + f(|\Gamma_2|)), \quad (16)$$

where $|\cdot|$ is absolute value, $f(x) = \ln \frac{e^x + 1}{e^x - 1} = \ln(\coth(\frac{x}{2}))$, and notice that $f^{-1}(x) = f(x)$. An equivalent expression is

$\Gamma_1 \boxplus \Gamma_2 = 2 \tanh^{-1} \left(\tanh(\frac{\Gamma_1}{2}) \tanh(\frac{\Gamma_2}{2}) \right)$ [72], and in general,

$$\boxplus_{j=1}^w \Gamma_j := 2 \tanh^{-1} \left(\prod_{j=1}^w \tanh \frac{\Gamma_j}{2} \right). \quad (17)$$

To resolve all erasures (minimizing (11)) while satisfying the target syndrome, we define a check-satisfaction reward function for maximization:

$$S(\Gamma_1, \Gamma_2, \dots, \Gamma_{2n}) := \sum_{i=1}^m (-1)^{s_i} \boxplus_{j \in \mathcal{N}(i)} \Gamma_j. \quad (18)$$

Algorithm 2 presents MBP₂, performing a soft message-passing to approximate a solution for (6) by updating probabilities (LLRs). Specifically, it approximates Γ_j to $\ln \frac{\Pr(\mathbf{E}_j = 0 \mid \text{syndrome is } \mathbf{s})}{\Pr(\mathbf{E}_j = 1 \mid \text{syndrome is } \mathbf{s})}$ by maximizing (18) (Sec. IV A).

The check-to-variable messages $\Delta_{i \rightarrow j}$ are normalized by some $\alpha > 0$, like classical normalized BP [73, 74]. Typically, $\alpha \geq 1$ is chosen to suppress overestimated messages. Here, we also consider $\alpha < 1$ to enlarge the BP step-size to search more possible solutions. Larger step-size may cause divergence. Inspired by Hopfield nets [58–60], MBP uses fixed inhibition (12), adding memory effects to BP to improve convergence even with $\alpha < 1$ [57] (see Appendix E 2).

We can select a proper α value using GD optimization to maximize (18). Section IV A validates this by linking BP update rules with GD. Given the physical error rate p , we can determine α from a locally linear function of p using the continuity of the reward function (18) (see (22)–(27)). Furthermore, we introduce an optional step (13) to adjust the initial LLR Λ_j to have enough magnitude $|\Lambda_{\text{GD}}|$, ensuring enough update gradients in harmful stopping sets. This is performed whenever the updated LLR Γ_j for index j does not have enough magnitude (i.e., $|\Gamma_j| < |\Lambda_{\text{GD}}|$) after every T_{GD} iterations. We analyse the selection of parameter values in Appendix E 3 and choose $T_{\text{GD}} = 5$ and $|\Lambda_{\text{GD}}| = 0.25$.

In BP the message $\Delta_{i \rightarrow j}$ is typically computed by $\Delta_{i \rightarrow j} = (-1)^{s_i} \boxplus_{j' \in \mathcal{N}(i) \setminus \{j\}} \Gamma_{j' \rightarrow i}$. For efficiency, we compute it by

$$\Delta_{i \rightarrow j} = \Delta_i \boxminus \Gamma_{j \rightarrow i} := 2 \tanh^{-1} \left(\tanh \frac{\Delta_i}{2} / \tanh \frac{\Gamma_{j \rightarrow i}}{2} \right), \quad (19)$$

where $\Delta_i = (-1)^{s_i} \boxplus_{j \in \mathcal{N}(i)} \Gamma_{j \rightarrow i}$ is computed first and every $\Gamma_{j \rightarrow i} \neq 0$. This ensures $0 < |\Delta_i| < |\Gamma_{j \rightarrow i}|$ for numerical stability, which is guaranteed by the function $\text{soft}(\cdot)$ in (15). Compared to the typical computation, this reduces the BP complexity from $O(2n j_2 (j_2 - 1))$ to $O(2n j_2)$ per-iteration, where j_2 is the mean column-weight of \mathbf{H} .

Additionally, we observe that altering the message-update schedule can significantly improve decoding convergence for highly degenerate codes (see Appendix H).

As discussed earlier, we can select the α value from GD, but it is based on the reward function (18) and not necessarily optimal. First, the function in (18) is not concave and has vanishing gradients when encountering stopping sets, so a gradient-based step-size search does not ensure convergence. Second, directly using a large step-size may lead to oscillations and prevent the algorithm from converging. To mitigate this, we can test a list of decoders with step-sizes ranging from small to large step-sizes $(1/\alpha)$. Thus,

Algorithm 3 : AMBP₂

Input: The same as in Algorithm 2 but further with a sequence of real values $\alpha_1 > \alpha_2 > \dots > \alpha_\ell > 0$.

Initialization: Let $i = 1$.

MBP Step: Run MBP₂($H, \mathbf{s}, T_{\max}, \alpha_i, \{\Lambda_j\}$),

which returns an indicator “CONVERGE” or “FAIL” with an estimated $\hat{E} \in \{0, 1\}^{2n}$.

Adaptive Check:

- If the return indicator is “CONVERGE”, return “CONVERGE” (with $\alpha^* = \alpha_i$ and the estimated \hat{E});
 - Otherwise, let $i \leftarrow i + 1$; if $i > \ell$, return “FAIL”;
 - Otherwise, repeat from the MBP Step.
-

For erasure decoding, all MBP instances with different α values can run in parallel, halting all instances as soon as one finds a feasible solution.

we also propose an adaptive MBP₂ (AMBP₂), as in Algorithm 3, which tests a list of $\alpha_1 > \dots > \alpha_\ell$ and adaptively select a proper α^* .

E. MBP₄, and unified (A)MBP_q notation, $q = 2$ or 4

We also consider quaternary BP (BP₄). This BP leverages the correlation between bits j and $j + n$ via the Pauli check matrix $H \in \{I, X, Y, Z\}^{m \times n}$ for error correction, enhancing accuracy in both classical and quantum settings [75], [61], when compared to binary BP. Indirectly, this can be interpreted as a turbo update between the two error components ($E^X | E^Z$) [76], reducing the likelihood of the decoder being halted by binary stopping sets in either the X or Z portion. Preliminary simulations show very good accuracy, so we do not design a GD step for quaternary BP.

For quaternary BP in the quantum setting, we express the variable-to-check ($j \rightarrow i$) message, following [61, 77], as

$$\ln \frac{\Pr(\text{Pauli error } E_j \text{ and entry } H_{ij} \text{ commute})}{\Pr(\text{Pauli error } E_j \text{ and entry } H_{ij} \text{ anti-commute})}, \quad (20)$$

$$\text{e.g., } = \ln \frac{p_j^I + p_j^X}{p_j^Y + p_j^Z} \text{ for initial LLR } (j \rightarrow i) \text{ if } H_{ij} = X. \quad (21)$$

Extending the derivations in Sec. IV A, we obtain quaternary MBP (MBP₄) and its adaptive version (AMBP₄); see [57].

Given a Pauli check matrix $H \in \{I, X, Y, Z\}^{m \times n}$, which uniquely determines a binary check matrix $\mathbf{H} \in \{0, 1\}^{m \times 2n}$, we consider a unified (A)MBP notation: let $\ell = 1$ for MBP and $\ell > 1$ for AMBP, and refer the decoder by

$$(\text{A})\text{MBP}_q(H, \mathbf{s}, T_{\max}, \{p_j^I, p_j^X, p_j^Y, p_j^Z\}_{j=1}^n, \{\alpha_i\}_{i=1}^\ell),$$

with $q = 4$ for (A)MBP₄ and $q = 2$ for (A)MBP₂. We state a unified (A)MBP_q algorithm in Algorithm 4.

For (A)MBP₂, if the optional GD step is applied, we refer the algorithm as GD (A)MBP₂ in simulations.

Algorithm 4 : Erasure decoding with (A)MBP_q, $q = 2$ or 4

Input:

A check matrix $H \in \{I, X, Y, Z\}^{m \times n}$, a syndrome $\mathbf{s} \in \{0, 1\}^m$, erased coordinates $\mathfrak{r} \subseteq \{1, 2, \dots, n\}$, an integer $T_{\max} > 0$, and a set of real $\alpha_1 > \alpha_2 > \dots > \alpha_\ell > 0$.

Include T_{GD} and $|\Lambda_{\text{GD}}|$ if the GD step is applied to (A)MBP₂.

Initialization.

- Set $(p_j^I, p_j^X, p_j^Y, p_j^Z) = (\frac{1}{4}, \frac{1}{4}, \frac{1}{4}, \frac{1}{4})$ for $j \in \mathfrak{r}$ and $(p_j^I, p_j^X, p_j^Y, p_j^Z) = (1, 0, 0, 0)$ for $j \in \bar{\mathfrak{r}}$. (Convert to binary distributions (14) if $q = 2$.)

Decoding.

- Run (A)MBP_q($H, \mathbf{s}, T_{\max}, \{p_j^I, p_j^X, p_j^Y, p_j^Z\}_{j=1}^n, \{\alpha_i\}_{i=1}^\ell$), with optional GD step with input $(T_{\text{GD}}, |\Lambda_{\text{GD}}|)$ if applied, and obtain an estimate $\hat{E} \in \{I, X, Y, Z\}^n$.

Output.

- Return $\hat{E} \in \{0, 1\}^{2n}$ and $\hat{\mathbf{s}} = \langle \hat{E}, H \rangle$, where \hat{E} and H are the binary version of \hat{E} and H , respectively.
-

III. DISCUSSIONS

We analysed the general erasure decoding problem, and proposed efficient decoders suitable for this task. Topological codes were known to achieve capacity with vanishing code rate [13–15]. We construct various rate bicycle and LP codes, and their MLD thresholds attain the erasure capacity (Fig. 2). Soft (A)MBP decoders behave like MLD at low logical error rate, achieving near-capacity performance with a small gap. The GD flipping decoder performs well on bicycle and LP codes, despite its extremely low complexity.

Our results extend beyond erasure errors. We apply our results on concatenated QLDPC codes with permutation-invariant (PI) codes [62, 63, 78–82] as inner codes. Deletion errors can be catastrophic for stabilizer codes, but PI codes can correct them [63, 83]. Unlike erasures, a primary challenge of deletion errors is the lack of error location information, making decoding more difficult, as misidentifying even one location can cause failure. Accurately locating all deletions to obtain erasures aids decoding but is time-consuming, increasing the physical error rate. Thus, accepting imperfect erasure conversions, where some leakage errors remain as localized deletions, can be more effective. We assume a local deletion model where each block of ℓ physical qubits has an identifiable boundary, protected by an $[[\ell, 1]]$ PI code, converting deletions into erasures. Figure 4 shows the deletion-to-erasure conversion performance in a channel with deletion probability ϵ , using a PI code that corrects t deletions (see legend). The $[[4, 1]]$ PI code [62, 84, 85] converts local deletions with probability $\epsilon = 0.385$ into erasure errors of rate $p < 0.5$, which topological codes can handle. At $\epsilon = 0.1$, an $[[\ell, 1]]$ code with $\ell < 15$ achieves a converted $p < 0.1$, allowing a QLDPC code rate above 3/4 (Fig. 2). In particular, if the per-qubit

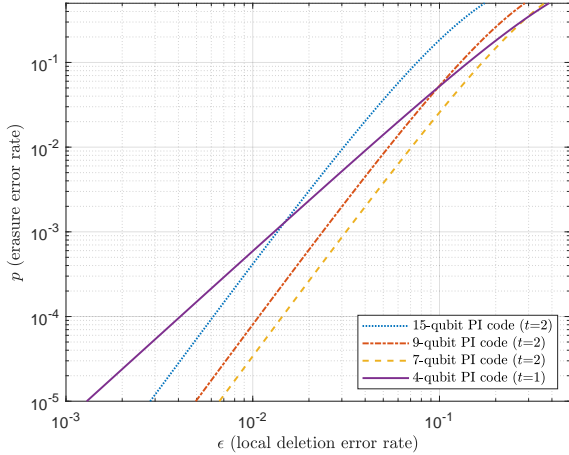


FIG. 4: Local deletion to erasure rate conversion using $[[\ell, 1]]$ PI codes for $\ell = 4, 7, 9, 15$ ([62, 85], [79], [78], [82]). The $[[4, 1]]$ PI code converts $\epsilon = 0.385$ to $p = 0.5$, which can then be handled by topological codes. At $\epsilon = 0.1$, an $[[\ell < 15, 1]]$ PI code achieves $p < 0.1$, allowing a QLDPC code rate above $3/4$ (Fig. 2). At $\epsilon = 0.01$, using a 7-qubit PI code achieves $p < 10^{-4}$, which allows QLDPC codes to attain a rate of essentially 1.

deletion probability is 0.01, then using a 7-qubit PI code can bring the logical erasure rate to below 10^{-4} , which allows QLDPC codes to attain a rate of essentially 1, which is close to the maximum possible rate.

In a large system, after converting dominant noise into erasures at known locations, we model additional errors that occur as qubit depolarizing errors. This mixed error model is discussed in [86] using peeling on 2D codes. In contrast, (A)MBP can decode general QLDPC codes in this error model. We show this using a $[[1054, 140]]$ LP code (see [18] or Appendix G 4) with the simulation setup in Sec. IV B. With (A)MBP₄, we adapt by adjusting the initial error distribution for the non-erased qubits to $(p^I, p^X, p^Y, p^Z) = (1 - p_0, \frac{p_0}{3}, \frac{p_0}{3}, \frac{p_0}{3})$, where p_0 can be set to either the depolarizing error rate p_{dep} or a suitable fixed value $< p_{\text{dep}}$ [57, 87]. With (A)MBP₂, the initial error distribution is $(p^{(0)}, p^{(1)})$, where $p^{(1)} = p^X + p^Y = p^Z + p^Y$ and $p^{(0)} = 1 - p^{(1)}$. The adjustment enables soft BP decoders to simultaneously correct both erasure and depolarizing errors. Figure 5 shows our decoder accuracy, assuming $p_{\text{dep}} = 0.01$. GD Flip-BP₂ cannot handle depolarizing errors, so we use MBP₂ with $\alpha = 1$ as a soft extension. All decoders successfully handle mixed errors. Among them, AMBP₄ shows the best accuracy, as depolarizing errors exhibit strong correlations between X and Z errors.

Our findings highlight the proposed decoders' adaptability and accuracy in handling various error types, including erasures, deletions, and depolarizing errors. Moreover, our methods extend to noisy syndrome extractions [88] and circuit-level noise [89]. We expect the versatility and high performance of our proposed decoders to help unlock the full potential of quantum LDPC codes, to accelerate the development of future fault-tolerant quantum computations.

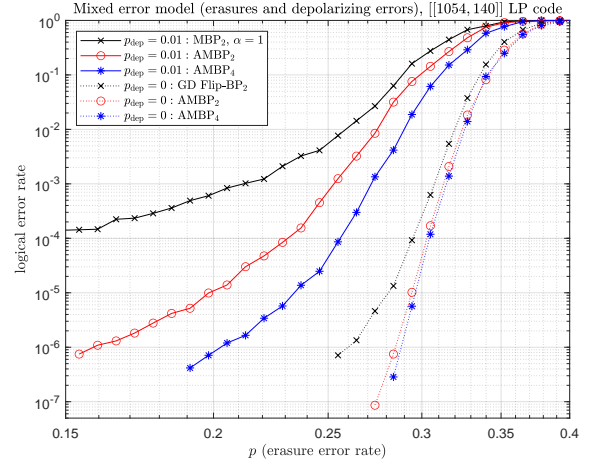


FIG. 5: BP accuracy for mixed erasure and depolarizing errors using the $[[1054, 140]]$ LP code. The curves with only erasure errors are provided for reference ($p_{\text{dep}} = 0$). AMBP₄ maintains strong accuracy in the mixed error model ($p_{\text{dep}} = 0.01$).

IV. METHODS

A. BP update rules and the relation with GD

For BP₂ syndrome decoding in the erasure channel, we have to satisfy two constraints, \mathfrak{r} and \mathfrak{s} (i.e., the erasure locations and the syndrome). The erasure information \mathfrak{r} is embedded in the initial distributions (14). The syndrome information \mathfrak{s} is included in BP₂ to update the initial LLR $\Lambda_j = \ln \frac{\Pr(E_j=0)}{\Pr(E_j=1)}$ to $\Gamma_j = \ln \frac{\Pr(E_j=0 \mid \text{syndrome is } \mathfrak{s})}{\Pr(E_j=1 \mid \text{syndrome is } \mathfrak{s})}$ for each binary error E_j for $j = 1, 2, \dots, 2n$. It is well-known that normalized BP₂ [73, 74] provides an efficient computation

$$\Gamma_j = \Lambda_j + \frac{1}{\alpha} \sum_{i \in \mathcal{M}(j)} (-1)^{s_i} 2 \tanh^{-1} \left(\prod_{j' \in \mathcal{N}(i) \setminus \{j\}} \tanh \frac{\Gamma_{j'}}{2} \right) \quad (22)$$

$$= \Lambda_j + \frac{1}{\alpha} \sum_{i \in \mathcal{M}(j)} \Delta_{i \rightarrow j} \quad (23)$$

like Algorithm 2. We justify this computation for the first iteration, with $\alpha = 1$, in Appendix E 1.

To determine the value of α in Algorithm 2, we relate BP to GD [57, 90]. Define the satisfaction at check node i as $(-1)^{s_i} 2 \tanh^{-1} \left(\prod_{j \in \mathcal{N}(i)} \tanh \frac{\Gamma_j}{2} \right)$. Summing this for all check nodes, we get the reward function (18), which is:

$$S(\Gamma_1, \dots, \Gamma_{2n}) = \sum_{i=1}^m (-1)^{s_i} 2 \tanh^{-1} \left(\prod_{j \in \mathcal{N}(i)} \tanh \frac{\Gamma_j}{2} \right). \quad (24)$$

Then

$$\frac{\partial S}{\partial \Gamma_j} = \sum_{i \in \mathcal{M}(j)} g_{ij} (-1)^{s_i} \prod_{j' \in \mathcal{N}(i) \setminus \{j\}} \tanh \frac{\Gamma_{j'}}{2}, \quad (25)$$

where g_{ij} is a positive term, as a function of $(\Gamma_1, \dots, \Gamma_{2n})$, as

$$g_{ij}(\Gamma_1, \dots, \Gamma_{2n}) = \frac{1 - \tanh^2 \frac{\Gamma_j}{2}}{1 - \left(\prod_{j' \in \mathcal{N}(i)} \tanh \frac{\Gamma_{j'}}{2} \right)^2} > 0. \quad (26)$$

Notice that $|\Gamma_{j \rightarrow i}| < \infty$ due to the use of $\text{soft}(\cdot)$ in (15). For non-erased part, $\Lambda_j = +\infty$, enforcing $\Gamma_j = \Lambda_j$ in (22) and fixing bit j decision as 0. For erased part, $\Lambda_j = 0$ in (22), so the other term determines the decision of bit j . Comparing this term in (22) and (25), and noting that $\tanh^{-1}(\cdot)$ and $g_{ij} > 0$ (as a multiplier) preserve the sign, we conclude that for BP, we should choose an α value such that

$$\frac{1}{\alpha} 2 \tanh^{-1} \left(\prod_{\substack{j' \in \mathcal{N}(i) \\ j' \neq j}} \tanh \frac{\Gamma_{j' \rightarrow i}}{2} \right) \propto g_{ij} \prod_{\substack{j' \in \mathcal{N}(i) \\ j' \neq j}} \tanh \frac{\Gamma_{j'}}{2} \quad (27)$$

to minimize (24). Using (27), we can express α as a locally linear function of p . A proper initial α value from p notably reduces AMBP iteration count (Sec. IV E).

We determine α by associating Γ_j with the physical error rate p . This step is crucial to prevent wrong decisions in the first iteration that would propagate incorrect information in subsequent iterations. As all functions in (27) are continuous, α is locally linear in Γ_j . Associating Γ_j with the channel error rate p , we express α as a locally linear function of p . We also associate α with the GD parameters in Algorithm 2 and obtain $T_{\text{GD}} = 5$ and $|\Lambda_{\text{GD}}| = 0.25$ for enough gradients for algorithm updates. See Appendix E 3.

B. Simulation setup

We conduct computer simulations for HP and GHP codes [50], [56], bicycle codes [17], LP codes [18], and topological toric and XZZX codes [44–46], [47–49]. Appendix G provides more information about the codes. We test BP and MLD on these codes.

For our BP decoders, we set $T_{\text{max}} = 100$. The average iteration count scales as $O(\log \log n)$ at relevant error rates, as discussed later. For (A)MBP unless otherwise stated, we use the group random schedule (Appendix H), and select α^* from 1.2, 1.19, \dots , 0.3 is using adaptive scheme.

C. A sphere-packing bound for accuracy evaluation

We aim for correcting t erasures with $t \propto n$. If a qubit is erased, it encounters I, X, Y , or Z with equal probability $1/4$. Using (2), a qubit encounters I with probability $1 - p + \frac{p}{4} = 1 - \frac{3}{4}p$, and encounters X, Y , or Z with equal probability $\frac{p}{4}$. Thus, before specifying \mathfrak{r} , we have

$$(p^I, p^X, p^Y, p^Z) = \left(1 - \frac{3p}{4}, \frac{p}{4}, \frac{p}{4}, \frac{p}{4}\right). \quad (28)$$

When $t \propto n$ are both large, we expect most occurred errors $E \in \{I, X, Y, Z\}^n$ to have approximately $\frac{3}{4}t$ components as X, Y , or Z . The probability that the number of such components deviates from $\frac{3}{4}t$ by δt for any $\delta > 0$ is exponentially suppressed in $t \propto n$.

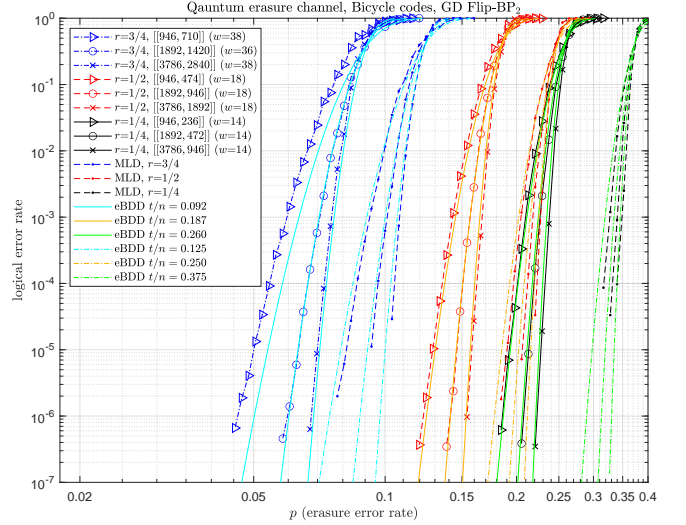


FIG. 6: Accuracy of GD Flip-BP₂ and MLD on bicycle codes. Decoders (A)MBP_q have accuracy comparable to GD Flip-BP₂ on these codes. BP threshold for rate 1/4 can be improved from 0.26 to 0.285 by using row-weight $w = 12$ (Appendix G 3).

Definition 3. The logical error rate of erasure bounded-distance-decoding (eBDD) with parameters n, t , and p is

$$P_{\text{eBDD}}(n, t, p) := \sum_{j=\lceil \frac{3}{4}t \rceil + 1}^n \binom{n}{j} \left(\frac{3}{4}p\right)^j \left(1 - \frac{3}{4}p\right)^{n-j}. \quad (29)$$

If a code family has decoding accuracy closely matching $P_{\text{eBDD}}(n, t, p)$ with a constant $\frac{t}{n} = p_{\text{th}}$ as n grows, then p_{th} serves an estimated threshold for the code family. With a fixed $\frac{t}{n} = p_{\text{th}}$ in (29), at any physical error rate $p < p_{\text{th}}$, the function $P_{\text{eBDD}}(n, t, p)$ decays exponentially as n increases. We discuss this in Appendix F. The accuracy estimated from eBDD is more reliable than the intersection of performance curves, particularly at low error rates (see Fig. 8).

D. Performance of capacity-achieving codes

We consider moderate-to-high-rate bicycle codes, low-rate LP codes, and vanishing-rate 2D topological codes. For bicycle and LP code families, we estimate the threshold values using eBDD, by comparing the decoder accuracy with (29) given fixed t/n .

First, we construct bicycle codes with rates $1/4, 1/2$, and $3/4$. A key step in bicycle construction is row-deletion, which requires heuristics [17], discussed in Appendix G 3. GD Flip-BP₂ suffices for decoding bicycle codes, with accuracy shown in Fig. 6, including MLD for comparison. Soft decoders (A)MBP have accuracy comparable to GD Flip-BP₂ on these codes. Using eBDD, we estimate the threshold values, as shown in the legend of Fig. 6. Bicycle codes exhibit capacity accuracy ($r = 1 - 2p$) with MLD threshold values at $p = 0.125, 0.25, 0.375$ for rates $r = 3/4, 1/2, 1/4$,

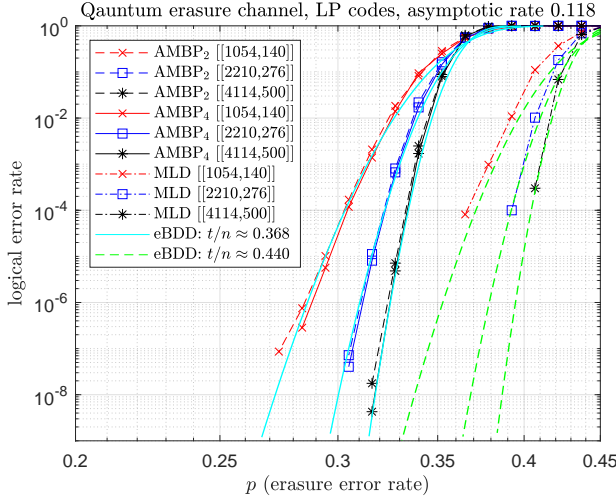


FIG. 7: Accuracy of AMBP and MLD on rate 0.118 LP codes. Our AMBP_q exhibit a threshold of $p_{\text{th}} = 0.368$. MLD curves suggest a higher threshold of $p_{\text{th}} = 0.44$. (For rate 0.04 case, see Fig. 20.)

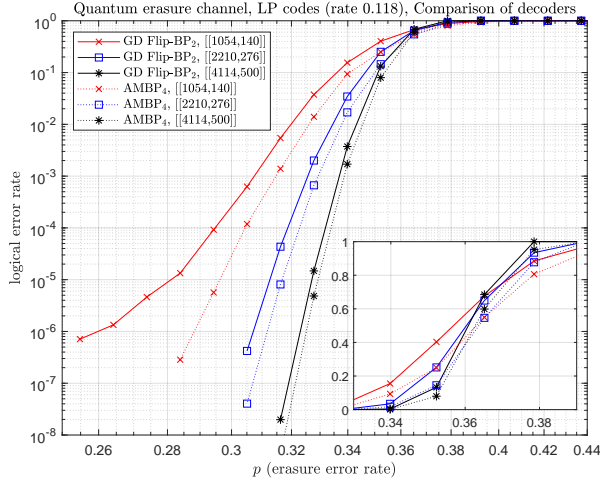


FIG. 8: GD Flip-BP₂ vs AMBP₄ on rate 0.118 LP codes. AMBP₄ has a threshold of 0.368 (Fig. 7). GD Flip-BP₂ closely matches AMBP₄ as n increases. Also note that good curve intersection does not guarantee accuracy at low error rates (red line).

respectively. The BP threshold follows closely, with a small gap at $p = 0.092, 0.187, 0.26$ for these rates. BP threshold for rate $1/4$ can be improved from 0.26 to 0.285 by using row-weight $w = 12$, by tolerating some error floor (see Appendix G 3).

Second, we construct quantum LP codes [18, Example 3] from classical quasi-cyclic (QC) matrices [26, 91, 92]. We construct LP code families with rates of 0.118 and 0.04. For rate 0.118, Figure 7 show the accuracy of AMBP and MLD, along with eBDD curves. LP codes exhibit strong accuracy with MLD, achieving a threshold of $p = 0.44$ at rate $r = 0.118$, closely matching the capacity $r = 1 - 2p$. AMBP decoders also achieve a large threshold of 0.368. For this code family, GD Flip-BP₂ performs almost as well as AMBP₄

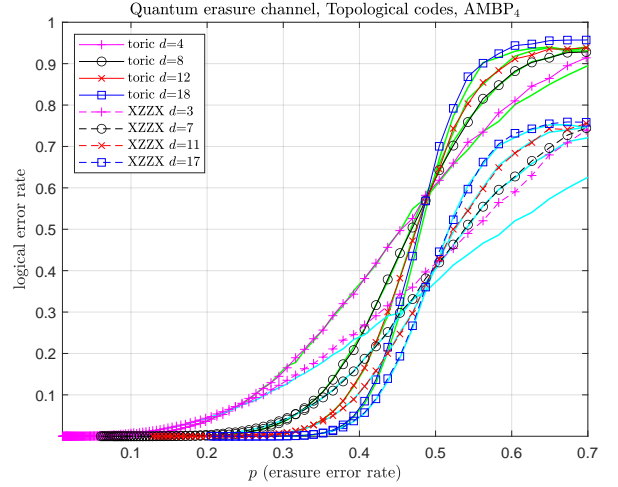


FIG. 9: Accuracy of AMBP₄ and MLD on toric and XZZX codes. Both decoders achieve a threshold of 0.5. MLD curves are shown in green and cyan for the toric and XZZX codes, respectively. Both decoders have the same accuracy at low error rates (Fig. 21).

when the code length increases, as shown in Fig. 8. This figure also indicate that good curve intersection does not guarantee accuracy at low error rates; see the red line.

Thresholds for the rate 0.04 LP codes are similarly estimated ($p_{\text{th}}^{(\text{BP})} = 0.405$ and $p_{\text{th}}^{(\text{MLD})} = 0.48$; see Appendix G 4).

GD Flip-BP₂ has very low implementation complexity, though its accuracy may depend on the code construction. Figures 6 and 8 show that it can achieve high accuracy with bicycle and LP constructions.

Third, for 2D topological codes, we consider (rotated) toric codes $[[L^2, 2, L]]$ for even L and (twisted) XZZX codes $[[((d^2 + 1)/2, 1, d)]]$ for odd d (see [44, 46], [47], or a summary of code structures in [93, Table I and figures]). For 2D codes, the intersection of performance curves, known as the Nishimori point, provides an estimate of the critical error probability (threshold) for MLD [45]. Among our decoders, AMBP₄ closely matches MLD accuracy for these codes, as shown in Fig. 9. Both decoders have a threshold of 0.5, consistent with [13–15]. For AMBP, we use a smaller $\alpha_1 = 0.95$ to increase the step-size, handling more erasures while maintaining decoder accuracy. To examine accuracy at low error rates, we replot Fig. 9 on a log scale, showing that AMBP₄ matches MLD (see Fig. 21 in Appendix G 5).

E. Selection of the α value

We demonstrate how to select a proper α value for MBP or an appropriate initial value α_1 for AMBP. A code with a transition point in the performance curve is convenient for this analysis. Consider the $[[882, 48, 16]]$ GHP code from [56]. The accuracy of MBP₂ with different α values is shown in Fig. 10. Three transition points occur around $p = 0.32, 0.33, 0.34$, for $\alpha = 1.2, 1.0, 0.8$, respectively. This locally linear trend aligns with our expecta-

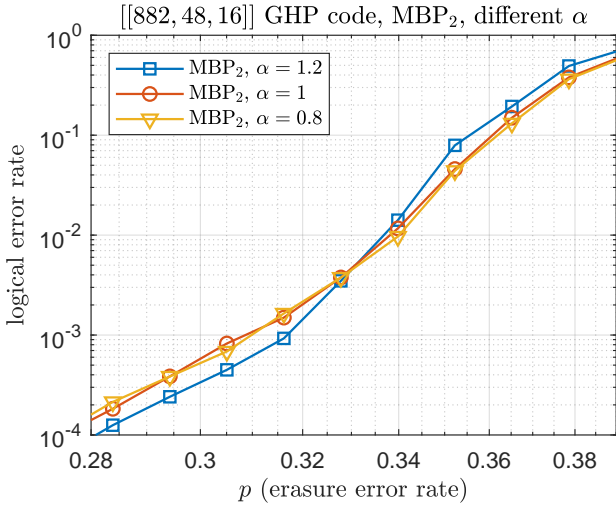


FIG. 10: Accuracy of MBP_2 on the $[[882, 48, 16]]$ GHP code. Three transition points occur around $p = 0.32, 0.33, 0.34$, for $\alpha = 1.2, 1.0, 0.8$, respectively, establishing a linear relation.

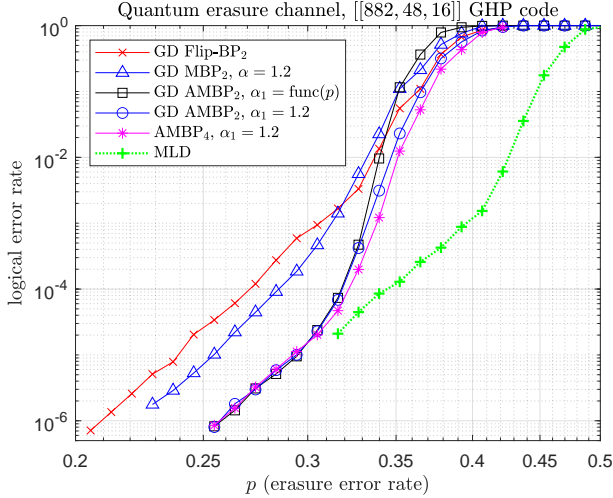


FIG. 11: Accuracy of several decoders on the $[[882, 48, 16]]$ GHP code. For BP decoders, AMBP-type decoders achieve the best accuracy, and can maintain a low iteration count when using $\alpha_1 = \text{func}(p)$ as in (32). The runtime is compared in Table II.

tion (Sec. IV A). We establish a linear relation by $(p, \alpha) =$

$(0.32, 1.2)$ and $(0.34, 0.8 + \text{margin})$, where the margin is 0.1 to prevent α from being too small. The obtained relation is: $\alpha = -15p + 6$. Hence, we propose a function:

$$\alpha = \text{func}(p) := \max(\min(-15p + 6, 1.2), 0.3), \quad (30)$$

where 1.2 and 0.3 are the upper and lower bounds, respectively. Additional simulations show that a wider range of α values does not lead to further improvement. With this α selection strategy (30), MBP achieves accuracy as the lower envelope of the curves in Fig. 10.

For AMBP-type decoders, we evaluate two strategies:

$$\alpha^* \in \{1.2, 1.19, \dots, 0.3\}, \quad \text{or} \quad (31)$$

$$\alpha^* \in \{\text{func}(p), \text{func}(p) - 0.01, \dots, 0.3\}. \quad (32)$$

We present the decoder accuracy in Fig. 11. As shown, the two strategies exhibit similar accuracy. Both strategies show similar average iteration counts when $p \leq 0.328$ (logical error rate $< 10^{-4}$), as detailed in Table II. A significant difference arises at higher error rates, such as $p = 0.392$. The strategy in (32) selects a proper α_1 for a given physical error rate p , making AMBP as efficient as MBP. An illustration of the two strategies is shown in Appendix (Fig. 16).

TABLE II: Average BP iteration counts for the $[[882, 48, 16]]$ GHP code. We include more decoders for reference than in Fig. 11. All BPs remain efficient at low error rates. For AMBP, two strategies (31) (fixed α_1) and (32) ($\alpha_1 = \text{func}(p)$) are compared, where (32) provides much faster runtime at high error rates.

average iteration counts	$p=0.255$	$p=0.328$	$p=0.392$
AMBP ₄ , $\alpha_1 = 1.2$	3.28	10.54	4628.89
AMBP ₄ , $\alpha_1 = \text{func}(p)$	3.28	8.33	90.27
MBP ₄ , $\alpha = 1.2$	3.27	6.14	80.12
GD AMBP ₂ , $\alpha_1 = 1.2$	3.30	11.98	5330.62
GD AMBP ₂ , $\alpha_1 = \text{func}(p)$	3.30	10.67	94.75
GD MBP ₂ , $\alpha = 1.2$	3.30	6.80	83.55
GD Flip-BP ₂	2.99	5.18	51.51

V. ACKNOWLEDGEMENTS

K.K. and Y.O. acknowledge support from EPSRC (Grant No. EP/W028115/1).

[1] D. Bluvstein, S. J. Evered, A. A. Geim, S. H. Li, H. Zhou, T. Manovitz, S. Ebadi, M. Cain, M. Kalinowski, D. Hangleiter, *et al.*, Logical quantum processor based on reconfigurable atom arrays, *Nature* **626**, 58 (2024).
 [2] P. Scholl, A. L. Shaw, R. B.-S. Tsai, R. Finkelstein, J. Choi, and M. Endres, Erasure conversion in a high-fidelity Rydberg quantum simulator, *Nature* **622**, 273 (2023).
 [3] S. Ma, G. Liu, P. Peng, B. Zhang, S. Jandura, J. Claes, A. P. Burgers, G. Pupillo, S. Puri, and J. D. Thompson, High-fidelity gates and mid-circuit erasure conversion in an atomic qubit, *Nature* **622**, 279

(2023).
 [4] Y. Wu, S. Kolkowitz, S. Puri, and J. D. Thompson, Erasure conversion for fault-tolerant quantum computing in alkaline earth Rydberg atom arrays, *Nat. Commun.* **13**, 4657 (2022).
 [5] I. Cong, H. Levine, A. Keesling, D. Bluvstein, S.-T. Wang, and M. D. Lukin, Hardware-efficient, fault-tolerant quantum computation with Rydberg atoms, *Phys. Rev. X* **12**, 021049 (2022).
 [6] A. Kubica, A. Haim, Y. Vaknin, H. Levine, F. Brandão, and A. Retzker, Erasure qubits: Overcoming the T_1 limit in superconducting circuits, *Phys. Rev. X* **13**, 041022 (2023).

- [7] J. D. Teoh, P. Winkel, H. K. Babla, B. J. Chapman, J. Claes, S. J. de Graaf, J. W. Garmon, W. D. Kalfus, Y. Lu, A. Maiti, *et al.*, Dual-rail encoding with superconducting cavities, *Proc. Nat. Acad. Sci. (PNAS)* **120**, e2221736120 (2023).
- [8] H. Levine, A. Haim, J. S. Hung, N. Alidoust, M. Kalaei, L. DeLorenzo, E. A. Wollack, P. Arrangoiz-Arriola, A. Khalajhedayati, R. Sanil, *et al.*, Demonstrating a long-coherence dual-rail erasure qubit using tunable transmons, *Phys. Rev. X* **14**, 011051 (2024).
- [9] M. Kang, W. C. Campbell, and K. R. Brown, Quantum error correction with metastable states of trapped ions using erasure conversion, *PRX Quantum* **4**, 020358 (2023).
- [10] C.-Y. Lu, W.-B. Gao, J. Zhang, X.-Q. Zhou, T. Yang, and J.-W. Pan, Experimental quantum coding against qubit loss error, *Proc. Natl. Acad. Sci. (PNAS)* **105**, 11050 (2008).
- [11] C. H. Bennett, D. P. DiVincenzo, and J. A. Smolin, Capacities of quantum erasure channels, *Phys. Rev. Lett.* **78**, 3217 (1997).
- [12] N. Delfosse and G. Zémor, Upper bounds on the rate of low density stabilizer codes for the quantum erasure channel, *Quantum Info. Comput.* **13**, 793–826 (2013).
- [13] T. M. Stace, S. D. Barrett, and A. C. Doherty, Thresholds for topological codes in the presence of loss, *Phys. Rev. Lett.* **102**, 200501 (2009).
- [14] M. Ohzeki, Error threshold estimates for surface code with loss of qubits, *Phys. Rev. A* **85**, 060301 (2012).
- [15] N. Delfosse and G. Zémor, Linear-time maximum likelihood decoding of surface codes over the quantum erasure channel, *Phys. Rev. Res.* **2**, 033042 (2020).
- [16] S. Bravyi, A. W. Cross, J. M. Gambetta, D. Maslov, P. Rall, and T. J. Yoder, High-threshold and low-overhead fault-tolerant quantum memory, *Nature* **627**, 778 (2024).
- [17] D. J. C. MacKay, G. Mitchison, and P. L. McFadden, Sparse-graph codes for quantum error correction, *IEEE Trans. Inf. Theory* **50**, 2315 (2004).
- [18] P. Panteleev and G. Kalachev, Quantum LDPC codes with almost linear minimum distance, *IEEE Trans. Inf. Theory* **68**, 213 (2022).
- [19] V. V. Williams, Multiplying matrices faster than Coppersmith-Winograd, in *Proc. Annu. ACM Symp. Theory Comput. (STOC)* (2012) pp. 887–898.
- [20] F. Le Gall, Powers of tensors and fast matrix multiplication, in *Proc. Int. Symp. Symb. Algebraic Comput.* (2014) pp. 296–303.
- [21] M. Sipser and D. A. Spielman, Expander codes, *IEEE Trans. Inf. Theory* **42**, 1710 (1996).
- [22] M. G. Luby, M. Mitzenmacher, M. A. Shokrollahi, and D. A. Spielman, Efficient erasure correcting codes, *IEEE Trans. Inf. Theory* **47**, 569 (2001).
- [23] C. Di, D. Proietti, I. E. Telatar, T. J. Richardson, and R. L. Urbanke, Finite-length analysis of low-density parity-check codes on the binary erasure channel, *IEEE Trans. Inf. Theory* **48**, 1570 (2002).
- [24] T. J. Richardson and R. L. Urbanke, Efficient encoding of low-density parity-check codes, *IEEE Trans. Inf. Theory* **47**, 638 (2001).
- [25] D. J. C. MacKay and M. S. Postol, Weaknesses of Margulis and Ramanujan-Margulis low-density parity-check codes, *Electron. Notes Theor. Comput. Sci.* **74**, 97 (2003).
- [26] R. M. Tanner, D. Sridhara, A. Sridharan, T. E. Fuja, and D. J. Costello, LDPC block and convolutional codes based on circulant matrices, *IEEE Trans. Inf. Theory* **50**, 2966 (2004).
- [27] A. Shokrollahi, Raptor codes, *IEEE Trans. Inf. Theory* **52**, 2551 (2006), see also <http://dx.doi.org/10.1561/01000000060>.
- [28] A. Zaidi, F. Athley, J. Medbo, U. Gustavsson, G. Durisi, and X. Chen, *5G Physical Layer: principles, models and technology components* (Academic Press, 2018).
- [29] K. Arora, J. Singh, and Y. S. Randhawa, A survey on channel coding techniques for 5G wireless networks, *Telecommun. Syst.* **73**, 637 (2020).
- [30] T. Richardson, Error floors of LDPC codes, in *Proc. Annu. Allerton Conf. Commun., Control, Comput.*, Vol. 41 (2003) pp. 1426–1435.
- [31] A. Orlitsky, R. Urbanke, K. Viswanathan, and J. Zhang, Stopping sets and the girth of Tanner graphs, in *Proc. IEEE Int. Symp. Inf. Theory (ISIT)* (2002) p. 2.
- [32] A. B. Alosious and P. K. Sarvepalli, Erasure decoding of two-dimensional color codes, *Phys. Rev. A* **100**, 042312 (2019).
- [33] H. M. Solanki and P. K. Sarvepalli, Decoding topological subsystem color codes over the erasure channel using gauge fixing, *IEEE Trans. Commun.* **71**, 4181 (2023).
- [34] S. Lee, M. Mhalla, and V. Savin, Trimming decoding of color codes over the quantum erasure channel, in *Proc. IEEE Int. Symp. Inf. Theory (ISIT)* (2020) pp. 1886–1890.
- [35] T. H. Cormen, C. E. Leiserson, R. L. Rivest, and C. Stein, *Introduction to algorithms* (MIT press, Cambridge, MA, 2009).
- [36] N. Connolly, V. Londe, A. Leverrier, and N. Delfosse, Fast erasure decoder for hypergraph product codes, *Quantum* **8**, 1450 (2024).
- [37] K. Sahay, J. Jin, J. Claes, J. D. Thompson, and S. Puri, High-threshold codes for neutral-atom qubits with biased erasure errors, *Phys. Rev. X* **13**, 041013 (2023).
- [38] J. Edmonds, Paths, trees, and flowers, *Can. J. Math.* **17**, 449 (1965).
- [39] M. Gökduman, H. Yao, and H. Pfister, Erasure decoding for quantum LDPC codes via belief propagation with guided decimation, in *Proc. Annu. Allerton Conf. Commun., Control, Comput.* (2024) pp. 1–8.
- [40] H. Yao, M. Gökduman, and H. D. Pfister, Cluster decomposition for improved erasure decoding of quantum LDPC codes, *arXiv preprint arXiv:2412.08817* (2024).
- [41] A. R. Calderbank and P. W. Shor, Good quantum error-correcting codes exist, *Phys. Rev. A* **54**, 1098 (1996).
- [42] A. M. Steane, Error correcting codes in quantum theory, *Phys. Rev. Lett.* **77**, 793 (1996).
- [43] S. B. Bravyi and A. Y. Kitaev, Quantum codes on a lattice with boundary, *arXiv preprint quant-ph/9811052* (1998).
- [44] A. Y. Kitaev, Fault-tolerant quantum computation by anyons, *Ann. Phys.* **303**, 2 (2003), preprint *arXiv: quant-ph/9707021* (1997).
- [45] E. Dennis, A. Kitaev, A. Landahl, and J. Preskill, Topological quantum memory, *J. Math. Phys.* **43**, 4452 (2002).
- [46] H. Bombin and M. A. Martin-Delgado, Optimal resources for topological two-dimensional stabilizer codes: Comparative study, *Phys. Rev. A* **76**, 012305 (2007).
- [47] A. A. Kovalev, I. Dumer, and L. P. Pryadko, Design of additive quantum codes via the code-word-stabilized framework, *Phys. Rev. A* **84**, 062319 (2011).
- [48] B. M. Terhal, F. Hassler, and D. P. DiVincenzo, From Majorana fermions to topological order, *Phys. Rev. Lett.* **108**, 260504 (2012).
- [49] J. Bonilla Ataides, D. Tuckett, S. Bartlett, S. Flammia, and B. Brown, The XZZX surface code, *Nat. Commun.* **12**, 1 (2021).
- [50] J.-P. Tillich and G. Zémor, Quantum LDPC codes with positive rate and minimum distance proportional to the square root of the block-length, *IEEE Trans. Inf. Theory* **60**, 1193 (2014).
- [51] A. A. Kovalev and L. P. Pryadko, Quantum Kronecker sum-product low-density parity-check codes with finite rate, *Phys. Rev. A* **88**, 012311 (2013).
- [52] D. Gottesman, Fault-tolerant quantum computation with constant overhead, *Quantum Inf. Comput.* **14**, 1338 (2014).
- [53] N. P. Breuckmann and J. N. Eberhardt, Quantum low-density parity-check codes, *PRX Quantum* **2**, 040101 (2021).
- [54] C.-Y. Lai and K.-Y. Kuo, Harnessing coding theory for reliable network quantum communication, *IEEE Wireless Commun.* **31**, 82 (2024).
- [55] D. Poulin and Y. Chung, On the iterative decoding of sparse quantum codes, *Quantum Inf. Comput.* **8**, 987 (2008).
- [56] P. Panteleev and G. Kalachev, Degenerate quantum LDPC codes with good finite length performance, *Quantum* **5**, 585 (2021).
- [57] K.-Y. Kuo and C.-Y. Lai, Exploiting degeneracy in belief propagation decoding of quantum codes, *npj Quantum Inf.* **8**, art. no. 111 (2022), (arXiv full version: <https://arxiv.org/abs/2104.13659>).
- [58] J. J. Hopfield, Neurons with graded response have collective computational properties like those of two-state neurons, *Proc. Nat. Acad. Sci. (PNAS)* **81**, 3088 (1984).
- [59] J. J. Hopfield and D. W. Tank, “neural” computation of decisions in optimization problems, *Biol. Cybern.* **52**, 141 (1985).
- [60] J. J. Hopfield and D. W. Tank, Computing with neural circuits: A model, *Science* **233**, 625 (1986).
- [61] K.-Y. Kuo and C.-Y. Lai, Refined belief propagation decoding of sparse-graph quantum codes, *IEEE J. Sel. Areas Inf. Theory* **1**, 487

- (2020).
- [62] Y. Ouyang, Permutation-invariant quantum codes, *Phys. Rev. A* **90**, 062317 (2014).
- [63] Y. Ouyang, Permutation-invariant quantum coding for quantum deletion channels, in *Proc. IEEE Int. Symp. Inf. Theory (ISIT)* (2021) pp. 1499–1503.
- [64] D. Wiedemann, Solving sparse linear equations over finite fields, *IEEE Trans. Inf. Theory* **32**, 54 (1986).
- [65] D. Bluvstein, H. Levine, G. Semeghini, T. T. Wang, S. Ebadi, M. Kalinowski, A. Keesling, N. Maskara, H. Pichler, M. Greiner, *et al.*, A quantum processor based on coherent transport of entangled atom arrays, *Nature* **604**, 451 (2022).
- [66] A. R. Calderbank, E. M. Rains, P. W. Shor, and N. J. A. Sloane, Quantum error correction via codes over $GF(4)$, *IEEE Trans. Inf. Theory* **44**, 1369 (1998).
- [67] D. Gottesman, *Stabilizer codes and quantum error correction*, Ph.D. thesis, California Institute of Technology, Pasadena, CA USA (1997).
- [68] R. G. Gallager, *Low-Density Parity-Check Codes*, no. 21 in Research Monograph Series (MIT Press, 1963).
- [69] R. Tanner, A recursive approach to low complexity codes, *IEEE Trans. Inf. Theory* **27**, 533 (1981).
- [70] J. Pearl, *Probabilistic reasoning in intelligent systems: networks of plausible inference* (Morgan Kaufmann, 1988).
- [71] D. J. C. MacKay, Good error-correcting codes based on very sparse matrices, *IEEE Trans. Inf. Theory* **45**, 399 (1999).
- [72] F. R. Kschischang, B. J. Frey, and H.-A. Loeliger, Factor graphs and the sum-product algorithm, *IEEE Trans. Inf. Theory* **47**, 498 (2001).
- [73] J. Chen and M. P. C. Fossorier, Density evolution for two improved BP-based decoding algorithms of LDPC codes, *IEEE Commun. Lett.* **6**, 208 (2002).
- [74] J. Chen, A. Dholakia, E. Eleftheriou, M. P. C. Fossorier, and X.-Y. Hu, Reduced-complexity decoding of LDPC codes, *IEEE Trans. Commun.* **53**, 1288 (2005).
- [75] M. Davey and D. MacKay, Low-density parity check codes over $GF(q)$, *IEEE Commun. Lett.* **2**, 165 (1998).
- [76] R. J. McEliece, D. J. C. MacKay, and J.-F. Cheng, Turbo decoding as an instance of Pearl’s “belief propagation” algorithm, *IEEE J. Sel. Areas Commun.* **16**, 140 (1998).
- [77] C.-Y. Lai and K.-Y. Kuo, Log-domain decoding of quantum LDPC codes over binary finite fields, *IEEE Trans. Quantum Eng.* **2**, art. no. 2103615 (2021).
- [78] M. B. Ruskai, Pauli exchange errors in quantum computation, *Phys. Rev. Lett.* **85**, 194 (2000).
- [79] H. Pollatsek and M. B. Ruskai, Permutationally invariant codes for quantum error correction, *Linear Algebra Appl.* **392**, 255 (2004).
- [80] Y. Ouyang and J. Fitzsimons, Permutation-invariant codes encoding more than one qubit, *Phys. Rev. A* **93**, 042340 (2016).
- [81] Y. Ouyang, Permutation-invariant qudit codes from polynomials, *Linear Algebra Appl.* **532**, 43 (2017).
- [82] A. Aydin, M. A. Alekseyev, and A. Barg, A family of permutationally invariant quantum codes, *Quantum* **8**, 1321 (2024).
- [83] T. Shibayama and M. Hagiwara, Permutation-invariant quantum codes for deletion errors, in *Proc. IEEE Int. Symp. Inf. Theory (ISIT)* (2021) pp. 1493–1498.
- [84] A. Nakayama and M. Hagiwara, The first quantum error-correcting code for single deletion errors, *IEICE Commun. Express* **9**, 100 (2020).
- [85] M. Hagiwara and A. Nakayama, A four-qubits code that is a quantum deletion error-correcting code with the optimal length, in *Proc. IEEE Int. Symp. Inf. Theory (ISIT)* (2020) pp. 1870–1874.
- [86] N. Delfosse and N. H. Nickerson, Almost-linear time decoding algorithm for topological codes, *Quantum* **5**, 595 (2021).
- [87] M. Hagiwara, M. P. C. Fossorier, and H. Imai, Fixed initialization decoding of LDPC codes over a binary symmetric channel, *IEEE Trans. Inf. Theory* **58**, 2321 (2012).
- [88] K.-Y. Kuo and C.-Y. Lai, Generalized quantum data-syndrome codes and belief propagation decoding for phenomenological noise, *IEEE Trans. Inf. Theory* **71**, 1824 (2025).
- [89] K.-Y. Kuo and C.-Y. Lai, Fault-tolerant belief propagation for practical quantum memory, *arXiv preprint arXiv:2409.18689* (2024).
- [90] R. Lucas, M. Bossert, and M. Breitbach, On iterative soft-decision decoding of linear binary block codes and product codes, *IEEE J. Sel. Areas Commun.* **16**, 276 (1998).
- [91] M. P. C. Fossorier, Quasi-cyclic low-density parity-check codes from circulant permutation matrices, *IEEE Trans. Inf. Theory* **50**, 1788 (2004).
- [92] G. A. Malema, *Low-density parity-check codes: construction and implementation*, Ph.D. thesis, University of Adelaide, SA, Australia (2007).
- [93] K.-Y. Kuo and C.-Y. Lai, Comparison of 2D topological codes and their decoding performances, in *Proc. IEEE Int. Symp. Inf. Theory (ISIT)* (2022) pp. 186–191.
- [94] M.-H. Hsieh and F. L. Gall, NP-hardness of decoding quantum error-correction codes, *Phys. Rev. A* **83**, 052331 (2011).
- [95] P. Iyer and D. Poulin, Hardness of decoding quantum stabilizer codes, *IEEE Trans. Inf. Theory* **61**, 5209 (2015).
- [96] K.-Y. Kuo and C.-C. Lu, On the hardnesses of several quantum decoding problems, *Quantum Inf. Process.* **19**, 1 (2020).
- [97] R. Cleve and D. Gottesman, Efficient computations of encodings for quantum error correction, *Phys. Rev. A* **56**, 76 (1997).
- [98] F. J. MacWilliams and N. J. A. Sloane, *The Theory of Error-Correcting Codes* (North-Holland Publishing Company, 1977).
- [99] W. Hoeffding, Probability inequalities for sums of bounded random variables, *J. Am. Stat. Assoc.* **13** (1963).
- [100] H. Chernoff, A measure of asymptotic efficiency for tests of a hypothesis based on the sum of observations, *Ann. Math. Stat.* **493** (1952).
- [101] K.-Y. Kuo and Y. Ouyang, Degenerate quantum erasure decoding, *arXiv preprint arXiv:2411.13509* (2024), (version 1).
- [102] N. Raveendran, N. Rengaswamy, F. Rozpedek, A. Raina, L. Jiang, and B. Vasić, Finite rate QLDPC-GKP coding scheme that surpasses the CSS Hamming bound, *Quantum* **6**, 767 (2022).
- [103] T. J. Richardson, M. A. Shokrollahi, and R. L. Urbanke, Design of capacity-approaching irregular low-density parity-check codes, *IEEE Trans. Inf. Theory* **47**, 619 (2001).
- [104] J. Du Crest, F. Garcia-Herrero, M. Mhalla, V. Savin, and J. Valls, Layered decoding of quantum LDPC codes, in *2023 12th Int. Symp. Top. Coding (ISTC)* (2023) pp. 1–5.

Appendix A: Stabilize coset structure and maximum-likelihood decoding

The decoding problem is tied to the stabilizer coset structure and probability. We first present two decoding strategies based on different optimization criteria [94–96].

Definition 4. (Classical-sense maximum-likelihood decoding (CMLD)) Given a binary check matrix $\mathbf{H} \in \{0, 1\}^{(n-k) \times 2n}$, a syndrome $\mathbf{s} \in \{0, 1\}^{n-k}$, and necessary information of the channel, where $\mathbf{s} = \langle \mathbf{E}, \mathbf{H} \rangle$ for some $\mathbf{E} \in \{0, 1\}^{2n}$ drawn from the channel model, a CMLD finds an $\hat{\mathbf{E}} \in \{0, 1\}^{2n}$ such that $\hat{\mathbf{E}} = \mathbf{E}$ with probability as high as possible.

The previous decoding criterion is not necessarily a true MLD criterion in the quantum case, as it relies on the classical criterion ($\hat{\mathbf{E}} = \mathbf{E}$) for successful error correction.

In the quantum case, two Pauli operators E and F have the same logical operation on the code space if they differ by a stabilizer. Their binary representations $\mathbf{E} = \varphi(E)$ and $\mathbf{F} = \varphi(F)$ satisfy $\mathbf{E} + \mathbf{F} \in C = \text{Row}(\mathbf{H})$, or equivalently, $\mathbf{F} \in \mathbf{E} + C$. In this case, we call \mathbf{F} a degenerate error of \mathbf{E} . Since \mathbf{E} and \mathbf{F} have to the same logical operation, we define the logical coset of \mathbf{E} as

$$\mathbf{E} + C = \{\mathbf{F} \in \{0, 1\}^{2n} : \mathbf{F} + \mathbf{E} \in C\}. \quad (\text{A1})$$

This leads us to consider:

Definition 5. (Quantum maximum-likelihood decoding (QMLD)): Given a binary check matrix $\mathbf{H} \in \{0, 1\}^{(n-k) \times 2n}$, a syndrome $\mathbf{s} \in \{0, 1\}^{n-k}$, and necessary information of the channel, where $\mathbf{s} = \langle \mathbf{E}, \mathbf{H} \rangle$ for some $\mathbf{E} \in \{0, 1\}^{2n}$ drawn from the channel model, a QMLD finds an $\hat{\mathbf{E}} \in \{0, 1\}^{2n}$ such that $\hat{\mathbf{E}} \in \mathbf{E} + C$ with probability as high as possible.

1. Coset structure of stabilizer codes

Let \mathcal{S} and $\mathcal{N}(\mathcal{S})$ be the stabilizer and its normalizer, respectively, in the n -fold Pauli group \mathcal{P}_n . The generators of $\mathcal{N}(\mathcal{S})$, which contains \mathcal{S} , have a simple representation [96, Sec. 4]. Using elementary row operations on the binary matrix (5) (together with equivalent transformations $X \leftrightarrow Z$ [66] used on selected qubits [96]), we obtain a standard form [96, 97] of the binary check matrix

$$\mathbf{H} = \left[\begin{array}{c|cc} \mathbf{1}_{n-k} & \mathbf{A} & \mathbf{B} \ \mathbf{C} \end{array} \right], \quad (\text{A2})$$

where $\mathbf{A}, \mathbf{C} \in \{0, 1\}^{(n-k) \times k}$ and $\mathbf{B} \in \{0, 1\}^{(n-k) \times (n-k)}$.

Recall that C is symplectic self-orthogonal, so it contains in its symplectic dual C^\perp , the image $\varphi(\mathcal{N}(\mathcal{S}))$ of the normalizer $\mathcal{N}(\mathcal{S})$. To find generators of C^\perp , we construct an $(n+k) \times 2n$ binary matrix \mathbf{G} by adding $2k$ rows to (A2):

$$\mathbf{G} = \left[\begin{array}{c|cc} \mathbf{1}_{n-k} & \mathbf{A} & \mathbf{B} \ \mathbf{C} \\ \mathbf{0} & \mathbf{1}_k & \mathbf{C}^T \ \mathbf{0} \\ \mathbf{0} & \mathbf{0} & \mathbf{A}^T \ \mathbf{1}_k \end{array} \right] = \left[\begin{array}{c} \mathbf{H} \\ \mathbf{L} \end{array} \right]. \quad (\text{A3})$$

It is easy to verify that \mathbf{G} has full row-rank and satisfies $\langle \mathbf{G}, \mathbf{H} \rangle = \mathbf{G}\mathbf{A}\mathbf{H}^T = \mathbf{0}$. Thus, $\text{Row}(\mathbf{G}) = C^\perp$ and we have

$$\varphi(\mathcal{N}(\mathcal{S})) = C^\perp = \text{Row}(\mathbf{G}).$$

By further adding $n-k$ binary vectors of length $2n$ to (A3), we form a $2n \times 2n$ matrix

$$\left[\begin{array}{c|cc} \mathbf{1}_{n-k} & \mathbf{A} & \mathbf{B} \ \mathbf{C} \\ \mathbf{0} & \mathbf{1}_k & \mathbf{C}^T \ \mathbf{0} \\ \mathbf{0} & \mathbf{0} & \mathbf{A}^T \ \mathbf{1}_k \\ \mathbf{0} & \mathbf{0} & \mathbf{1}_{n-k} \ \mathbf{0} \end{array} \right] = \left[\begin{array}{c} \mathbf{H} \\ \mathbf{L} \\ \mathbf{V} \end{array} \right] = \left[\begin{array}{c} \mathbf{G} \\ \mathbf{V} \end{array} \right]. \quad (\text{A4})$$

The rows in the matrix (A4) span the vector space $\{0, 1\}^{2n}$.

We describe the stabilizer coset structure. Observe that

$$C = \text{Row}(\mathbf{H}) \subseteq \text{Row}(\mathbf{G}) = C^\perp \subseteq \{0, 1\}^{2n}. \quad (\text{A5})$$

By (A5), together with (A4), we have a quotient group:

$$\{0, 1\}^{2n}/C^\perp = \{\mathbf{v} + C^\perp : \mathbf{v} \in \text{Row}(\mathbf{V})\}.$$

This partitions $\{0, 1\}^{2n}$ into 2^{n-k} non-overlapping error cosets, and each coset contains $|C^\perp| = 2^{n+k}$ vectors sharing the same syndrome. Distinct error cosets are identified by distinct error coset leaders in $\{\mathbf{v}^{(i)}\}_{i=1}^{2^{n-k}} = \text{Row}(\mathbf{V})$.

Similarly, by (A5), together with (A3) or (A4), we have another quotient group:

$$C^\perp/C = \{\boldsymbol{\ell} + C : \boldsymbol{\ell} \in \text{Row}(\mathbf{L})\}. \quad (\text{A6})$$

This partitions C^\perp into 2^{2k} non-overlapping logical cosets, and each logical coset contains $|C| = 2^{n-k}$ vectors. Distinct logical cosets in (A6) are identified by distinct logical coset leaders in $\{\boldsymbol{\ell}^{(j)}\}_{j=1}^{2^{2k}} = \text{Row}(\mathbf{L})$, where \mathbf{L} is in (A3) or (A4).

Like the classical standard array for decoding [98], we construct a quantum standard array for decoding [96]:

$$\left[\begin{array}{cccc} \mathbf{v}^{(1)} + \boldsymbol{\ell}^{(1)} + C & \mathbf{v}^{(1)} + \boldsymbol{\ell}^{(2)} + C & \dots & \mathbf{v}^{(1)} + \boldsymbol{\ell}^{(2^k)} + C \\ \mathbf{v}^{(2)} + \boldsymbol{\ell}^{(1)} + C & \mathbf{v}^{(2)} + \boldsymbol{\ell}^{(2)} + C & \dots & \mathbf{v}^{(2)} + \boldsymbol{\ell}^{(2^k)} + C \\ \vdots & \vdots & \ddots & \vdots \\ \mathbf{v}^{(2^{n-k})} + \boldsymbol{\ell}^{(1)} + C & \mathbf{v}^{(2^{n-k})} + \boldsymbol{\ell}^{(2)} + C & \dots & \mathbf{v}^{(2^{n-k})} + \boldsymbol{\ell}^{(2^k)} + C \end{array} \right]. \quad (\text{A7})$$

In (A7), there are 2^{n-k} rows, each representing an error coset with the same syndrome, and every row contains 2^{2k} logical cosets. (Examples are shown in Fig. 12.)

We introduce some notation used later. Given \mathbf{H} for a stabilizer code, we consider some occurred Pauli error $E \in \mathcal{P}_n$ with binary form $\varphi(E) = \mathbf{E}$ and syndrome $\mathbf{s}(E) = \langle \mathbf{E}, \mathbf{H} \rangle$. The error \mathbf{E} lies in the some coset $\mathbf{v}^{(i)} + \boldsymbol{\ell}^{(j)} + C$ located in (A7), which the decoder aims to identify. We denote the target $\mathbf{v}^{(i)}$ and $\boldsymbol{\ell}^{(j)}$ by $\mathbf{v}^{(\mathbf{s}(E))}$ and $\boldsymbol{\ell}^{(E)}$, respectively.

Note that $\mathbf{v}^{(\mathbf{s}(E))} = (\mathbf{0}, \mathbf{0} | \mathbf{s}, \mathbf{0})$ when \mathbf{H} is in the standard form (A2). However, calculating $\boldsymbol{\ell}^{(E)}$ is non-trivial.

2. Proof of Lemma 1 (a counting lemma)

Let $\mathfrak{r} \subseteq \{1, 2, \dots, n\}$ and $\mathbf{s} \in \{0, 1\}^{n-k}$ denote the erasure information and the syndrome, respectively. Let $\mathbf{E}, \mathbf{F} \in$

$\{0, 1\}^{2n}$ be two erasure- and syndrome-matched errors in different logical cosets $E + C \neq F + C$. Let

$$\{\tilde{E}\} := \{E' \in E + C : (E'_j^X | E'_j^Z) = (0|0) \forall j \in \bar{r}\},$$

which contains degenerate errors of E that are also erasure-matched. Using this representation, we have

$$\begin{aligned} \{\tilde{E}\} &\subseteq E + C = \mathbf{v}^{(s(E))} + \boldsymbol{\ell}^{(E)} + C, \text{ and} \\ \{\tilde{F}\} &\subseteq F + C = \mathbf{v}^{(s(F))} + \boldsymbol{\ell}^{(F)} + C, \end{aligned}$$

where we also use the notation mentioned after (A7). For this lemma, it suffices to prove $|\{\tilde{E}\}| = |\{\tilde{F}\}|$. Then we will have two equal probabilities $\Pr(E + C | \mathfrak{r}, \mathbf{s}) \propto |\{\tilde{E}\}|$ and $\Pr(F + C | \mathfrak{r}, \mathbf{s}) \propto |\{\tilde{F}\}|$ after discussing (A13), i.e., the two logical cosets $E + C$ and $F + C$ are equally good in probability.

By assumption, $\mathbf{s}(E) = \mathbf{s}(F)$ and we have that $E + C$ and $F + C$ differ by a vector $\boldsymbol{\ell}' = \boldsymbol{\ell}^{(E)} - \boldsymbol{\ell}^{(F)} \in \text{Row}(\mathbf{L})$, where \mathbf{L} is in (A4). For our purpose, we choose a difference vector $\boldsymbol{\ell} = E - F$. By our choice of $\boldsymbol{\ell}$, we have $(\boldsymbol{\ell}_j^X | \boldsymbol{\ell}_j^Z) = (0|0)$ for all $j \in \bar{r}$. (It is not necessary for $\boldsymbol{\ell}$ to equal to $\boldsymbol{\ell}'$, but they differ by a stabilizer, i.e., $\boldsymbol{\ell} - \boldsymbol{\ell}' \in C$.) With $\boldsymbol{\ell}$ as a mapping, the elements in $\{\tilde{E}\}$ are in one-to-one correspondence with the elements in $\{\tilde{F}\}$. Thus, $|\{\tilde{E}\}| = |\{\tilde{F}\}|$.

3. Maximum-likelihood decoding

Consider a stabilizer code with $\varphi(S) = C \subset \{0, 1\}^{2n}$. In MLD, the goal is to find an error estimate \hat{E} in a logical coset $\mathbf{v}^{(s(E))} + \boldsymbol{\ell}^{(E)} + C$ that maximizes the sum of the probabilities of its elements relative to other logical cosets. The syndrome $\mathbf{s} = \langle E, \mathbf{H} \rangle \in \{0, 1\}^{n-k}$ is given. For erasure decoding, we are also given the erasures $\mathfrak{r} \subseteq \{1, 2, \dots, n\}$.

Given a physical error rate p , the probability to obtain a certain erasure pattern \mathfrak{r} is

$$\Pr(\mathfrak{r}) = p^{|\mathfrak{r}|} (1-p)^{n-|\mathfrak{r}|}. \quad (\text{A8})$$

For an $E \in \{0, 1\}^{2n}$ (with corresponding $E \in \mathcal{P}_n$), according to the quantum erasure channel model, we have the conditional probability of E given \mathfrak{r} as

$$\Pr(E | \mathfrak{r}) = \begin{cases} (1/4)^{|\mathfrak{r}|}, & \text{if } E_j = I \forall j \in \bar{r}, \\ 0, & \text{otherwise.} \end{cases} \quad (\text{A9})$$

So all erasure-matched solutions are equally good before the syndrome is given.

Discussions in literature often state that all feasible solutions are equally good, after the syndrome is given. We show this mathematically. By Bayes' rule, the conditional probability of E given a certain \mathfrak{r} and \mathbf{s} is

$$\Pr(E | \mathfrak{r}, \mathbf{s}) = \frac{\Pr(E, \mathfrak{r}, \mathbf{s})}{\Pr(\mathfrak{r}, \mathbf{s})} \quad (\text{A10})$$

We have $\Pr(\mathfrak{r}, \mathbf{s}) > 0$ since the syndrome is produced from the erasure error, and it is a constant. The numerator in (A10) is either a constant or 0; to see this, rewrite (A10) as

$$\Pr(E | \mathfrak{r}, \mathbf{s}) = \frac{\Pr(\mathfrak{r}) \Pr(E | \mathfrak{r}) \Pr(\mathbf{s} | E, \mathfrak{r})}{\Pr(\mathfrak{r}, \mathbf{s})}. \quad (\text{A11})$$

The term $\Pr(\mathfrak{r})$ is a constant as in (A8). The term $\Pr(E | \mathfrak{r})$ is either a constant or 0 as in (A9). The term $\Pr(\mathbf{s} | E, \mathfrak{r})$ is either 1 or 0, depending on whether E is an erasure- and syndrome-matched error or not. Such an E is a feasible solution to (6). Consequently, we represent (A10) as

$$\Pr(E | \mathfrak{r}, \mathbf{s}) = \begin{cases} \text{a constant} \propto (1/4)^{|\mathfrak{r}|}, & \text{if } E \text{ satisfies } \mathfrak{r} \text{ and } \mathbf{s}, \\ 0, & \text{otherwise.} \end{cases} \quad (\text{A12})$$

The CMLD in Def. 4 aims to maximize (A10). As shown in (A12), all feasible solutions to (6) are equally good for this purpose. This leads to:

Lemma 4. *For decoding a stabilizer code, if erasures $\mathfrak{r} \subseteq \{1, 2, \dots, n\}$ and syndrome $\mathbf{s} \in \{0, 1\}^{n-k}$ are given for decoding, then any feasible solution to (6) maximizes $\Pr(E | \mathfrak{r}, \mathbf{s})$ and is an optimal solution for CMLD in Def. 4.*

In contrast, QMLD in Def. 5 aims to maximize the following conditional probability of a logical coset given \mathfrak{r} and \mathbf{s}

$$\Pr(E + C | \mathfrak{r}, \mathbf{s}) := \sum_{E' \in E + C} \Pr(E' | \mathfrak{r}, \mathbf{s}), \quad (\text{A13})$$

where $\Pr(E' | \mathfrak{r}, \mathbf{s})$ is either a positive constant or 0 by (A12). This result, together with the counting lemma (Lemma 1), we establish Theorem 2 in the main text.

4. Coset structure example and decoding failure types

We illustrate the coset structure in Fig. 12, using the two error cases in Example 1. The first error case is simple. The second error case allow us to discuss two types of failures (non-convergence or false convergence).

When a decoder outputs an estimate \hat{E} for an error E with syndrome \mathbf{s} , we have either convergence ($\langle \hat{E}, \mathbf{H} \rangle = \mathbf{s}$) or non-convergence ($\langle \hat{E}, \mathbf{H} \rangle \neq \mathbf{s}$). Convergence further splits into two cases: successful decoding ($\langle \hat{E}, \mathbf{H} \rangle = \mathbf{s}, \hat{E} \in E + C$) or false convergence ($\langle \hat{E}, \mathbf{H} \rangle = \mathbf{s}, \hat{E} \notin E + C$). Thus:

$$\begin{aligned} \text{logical error rate} &= \text{non-convergence rate} + \text{false convergence rate}, \\ \Pr(\hat{E} \notin E + C) &= \Pr(\langle \hat{E}, \mathbf{H} \rangle \neq \mathbf{s}) + \Pr(\langle \hat{E}, \mathbf{H} \rangle = \mathbf{s}, \hat{E} \notin E + C). \end{aligned} \quad (\text{A14})$$

MLD always finds a feasible solution (matching \mathfrak{r} and \mathbf{s}) and fails only in false convergence.

We present two results for evaluating if an erasure decoder achieves MLD. For an ‘‘erasure decoder’’ we assume its output always matches \mathfrak{r} , which is trivially achieved by setting non-erased bit estimates to 0, like our BP (Remark 3).

Lemma 5. *An erasure decoder is an MLD if and only if it always finds a feasible solution to (6) (matching \mathfrak{r} and \mathbf{s}). Alternatively, an erasure decoder is an MLD if and only if it exhibits identical logical error and false convergence rates.*

Proof. The first statement follows from Theorem 2. For the second statement, only the converse is non-trivial. As an erasure decoder always matches \mathfrak{r} , identical logical error and false convergence rates imply that the output always match \mathbf{s} by (A14). Thus, the decoder is an MLD by the first statement. \square

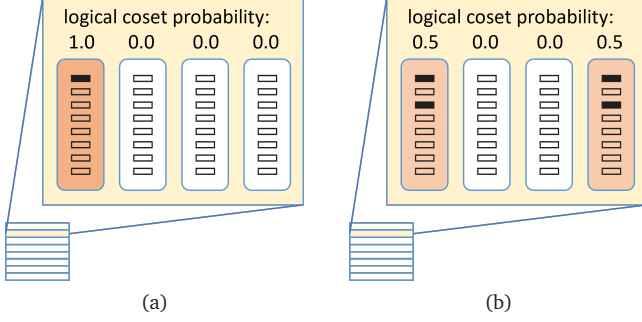


FIG. 12: Coset structure and logical coset probability for the $[[4, 1]]$ code in Example 1, given syndrome $\mathbf{s} = (0, 1, 0)$ and erasures (a) $\mathfrak{r} = \{2\}$ or (b) $\mathfrak{r} = \{2, 4\}$. The structure here follows the quantum standard array (A7)^a. An MLD always finds a feasible solution (a black bar), but false convergence may occur^b.

^a Each subfigure shows $2^{n-k} = 8$ error cosets, with the zoomed coset (the 2nd row) matching the syndrome $\mathbf{s} = (0, 1, 0)$. Every error coset contains $2^{2k} = 4$ logical cosets, each with $2^{n-k} = 8$ errors. Errors are depicted as bars, with positive and equal probability errors (feasible solutions) shown in black. Logical cosets with feasible solutions contain the same number of feasible solutions. In (b), four feasible solutions (each with probability 0.25) are equally distributed in the 1st and 4th logical cosets, resulting in a probability of 0.5 for each coset.

^b In (b), if the actual error lies in the 1st (logical) coset but the decoder output is in the 4th coset, then false convergence occurs (cf. (A14)).

Corollary 6. *If an erasure decoder has approximate logical error and false convergence rates, then it performs closely to MLD. The decoder's false convergence rate provides a lower bound for the logical error rate of MLD, with accuracy depending on simulation precision.*

Lemma 5 and Corollary 6 provide a method to evaluate whether an erasure decoder achieves MLD, using simulation data alone, without requiring Gaussian decoder as an MLD reference. We also verify Lemma 5 and Corollary 6 through simulations (see Table III).

Appendix B: Solution uniqueness and distance properties

The code's minimum distance determines whether there is a unique solution to (7). We first define the minimum distance of a stabilizer code [66, 67]. For a Pauli $E \in \mathcal{P}_n$, let its weight $w(E)$ be the number of non-identity components. For its binary form $E = \varphi(E)$, define the *generalized weight* of E as $\text{gw}(E) = w(E)$. Given a stabilizer group $\mathcal{S} < \mathcal{P}_n$, its normalizer in \mathcal{P}_n is $\mathcal{N}(\mathcal{S}) = \{E \in \mathcal{P}_n : EF = FE \forall F \in \mathcal{S}\}$. Recall that $C = \varphi(\mathcal{S}) = \text{Row}(\mathbf{H})$ and $C^\perp = \varphi(\mathcal{N}(\mathcal{S})) = \{\mathbf{v} \in \{0, 1\}^{2n} : \langle \mathbf{v}, \mathbf{H} \rangle = 0\}$. Note that $\mathcal{S} < \mathcal{N}(\mathcal{S})$ and $C \subseteq C^\perp$. For an $[[n, k \geq 1]]$ stabilizer code, its minimum-distance is

$$d = \min\{\text{gw}(\mathbf{E}) : \mathbf{E} \in C^\perp \setminus C\}. \quad (\text{B1})$$

For $k = 0$, we have $C^\perp = C$. The minimum distance in this case is defined as

$$d' = \min\{\text{gw}(\mathbf{E}) : \mathbf{E} \in C^\perp \setminus \mathbf{0}\}. \quad (\text{B2})$$

We also define d' for $k \geq 1$. In general, $d' \leq d$. If $d' < d$, the code is a degenerate code. With large $d - d'$, the code has strong degeneracy (or say, the code is highly degenerate). If $d' = d$, the code is called a non-degenerate code, yet it still exhibits some degeneracy, as discussed earlier (A1).

We relate the uniqueness of the solution in (7) with the code's minimum distance. Similar to the classical coding theory [98], a non-zero vector \mathbf{E} with $\text{gw}(\mathbf{E}) \leq d' - 1$ always chooses a set of columns in \mathbf{H} that are linearly independent. Notice that in (6), \mathbf{s}^T (a column vector) is generated by columns of $\mathbf{H}\mathbf{A}$ (which are just columns of \mathbf{H}) using non-zero entries of \mathbf{E} . Hence, we have the following cases.

If $|\mathfrak{r}| \leq d' - 1$, the columns of $[\mathbf{H}_{\mathfrak{r}}^Z | \mathbf{H}_{\mathfrak{r}}^X]$ in (7) are linearly independent, and hence there is a unique solution $\hat{\mathbf{E}}$ to (7), which is the actual error, i.e., $\hat{\mathbf{E}} = \mathbf{E}$. As a consequence, an MLD always succeeds with $\hat{\mathbf{E}} = \mathbf{E}$ when $|\mathfrak{r}| \leq d' - 1$.

If $|\mathfrak{r}| \geq d'$, the columns of $[\mathbf{H}_{\mathfrak{r}}^Z | \mathbf{H}_{\mathfrak{r}}^X]$ in (7) may be linearly dependent, leading to multiple solutions for (7). We divide this scenario into two cases as follows.

First, if $d' \leq |\mathfrak{r}| \leq d - 1$, then (7) has solutions that lie in the same logical coset containing the actual error. This follows from (B1) and (B2), which ensure that any solution $\hat{\mathbf{E}}$ to (7), if different from the actual error \mathbf{E} , differs only by a stabilizer. Hence, $\hat{\mathbf{E}}$ and \mathbf{E} lie in the same logical coset. As a consequence, an MLD always succeeds with $\hat{\mathbf{E}} \in \mathbf{E} + C$ when $d' \leq |\mathfrak{r}| \leq d - 1$.

Second, if $|\mathfrak{r}| \geq d$, then an error \mathbf{E} may cause (7) to have multiple solutions spanning in two or more logical cosets. However, if the majority of occurring errors do not lead to this unwanted span, the decoding failure rate remains low. For example, this advantage is evident in classical LDPC codes [23, 68] and quantum LDPC codes [17, 36].

Appendix C: Stopping sets and Tanner graph girth

Recall that a Tanner graph induced by an $m \times 2n$ binary matrix \mathbf{H} is a bipartite graph consisting of m check nodes and $2n$ binary variable nodes (Fig. 3). An edge connects check node i and variable node j if $\mathbf{H}_{ij} = 1$. Also, when $\mathbf{H}_{ij} = 1$, we say that row i checks column j . We define the concept of stopping sets by considering the binary check matrix \mathbf{H} of a binary code C of length $2n$.

Definition 6. (Stopping sets) [23, 25–27, 30, 31] *Let $\text{ST} \subseteq \{1, 2, \dots, 2n\}$. The subset ST is a stopping set of a binary check matrix \mathbf{H} if, for every row of \mathbf{H} , the row either checks no variable from ST or checks at least two variables from ST .*

When a stabilizer code of length n is described as a binary code of length $2n$, the quantum erasure decoding problem, by solving linear equations (6), is like a classical erasure decoding problem [22, 36]. For efficiency, Flip-BP₂ is usually conducted for decoding, which passes messages on a Tanner graph like Fig. 3(a) [22–27]. This decoder performs iterative *bit-flipping* to flip unknown bits in (6) to find a feasible solution. In Flip-BP₂, a bit is chosen to flip if it is a single unknown variable (bit) in a check. However, Flip-BP₂ may easily terminate before finding a feasible solution, if

the code contains small stopping sets [23–27, 30, 31]. This prevents the decoder from converging.

Example 2. Consider the binary \mathbf{H} in (8),

$$\mathbf{H} = [\mathbf{H}^X | \mathbf{H}^Z] = \begin{bmatrix} 1 & 0 & 0 & 0 & | & 0 & 0 & 1 & 0 \\ 0 & 1 & 0 & 1 & | & 0 & 1 & 0 & 1 \\ 0 & 0 & 1 & 1 & | & 1 & 0 & 0 & 1 \end{bmatrix}. \quad (\text{C1})$$

The coordinates of error variables \mathbf{E}_4^X and \mathbf{E}_4^Z form a stopping set. If the fourth qubit is erased ($\mathfrak{r} = \{4\}$) and results in Pauli error $E = I \otimes I \otimes I \otimes Y$, then Flip-BP₂ stops before finding a feasible solution. The matrix \mathbf{H} restricted to $\mathfrak{r} = \{4\}$ is $[\mathbf{H}_\mathfrak{r}^X | \mathbf{H}_\mathfrak{r}^Z] = \begin{bmatrix} 0 & | & 0 \\ 1 & | & 1 \end{bmatrix}$.

The length of the shortest cycle in a graph is called *girth*. The size of the smallest stopping set of a code is called *stopping number*. We present Remarks 7 and 8, based on [31].

Remark 7. For classical LDPC matrices of constant column-weight at least 3, the stopping number grows significantly with the girth.

QLDPC codes can be constructed from classical codes with favourable girth properties, such as LP codes based on QC matrices with large girth. However, predicting the resultant girth is challenging and requires further study.

Remark 8. The stopping number lower bounds the classical minimum distance of the code. Thus, a small classical minimum distance imposes a small stopping number².

Example 3. In Example 2, the restricted matrix $[\mathbf{H}_\mathfrak{r}^X | \mathbf{H}_\mathfrak{r}^Z]$ has a submatrix $\begin{bmatrix} 1 & | & 1 \\ 1 & | & 1 \end{bmatrix}$, which forms a four-cycle in the Tanner graph. A four-cycle is a cycle of shortest length. By treating \mathbf{H} in (C1) as a parity-check matrix of a classical code of length 8, the code has small girth 4. Note that the code has a classical minimum distance 2, and its stopping number is 2.

Stabilizer check matrices tend to contain short cycles [17, 55], resulting in small girth, which makes it difficult to support a large stopping number (Remark 7). Furthermore, if the check matrix is sparse, as in the case of QLDPC codes, it results in a small stopping number. For stabilizer codes, we have $C = \text{Row}(\mathbf{H}) \subseteq \text{Row}(\mathbf{G}) = C^\perp$. So a QLDPC code contains numerous small-weight classical codewords in C^\perp due to the low density of \mathbf{H} . This causes a small classical distance of C^\perp and hence a small stopping number (Remark 8). This leads to the following dilemma:

Remark 9. We aim for a QLDPC code with a binary check matrix \mathbf{H} as sparse as possible; however, the code's stopping number is upper bounded by the minimum row-weight of \mathbf{H} .

² This is not shown in [31] but follows from Appendix B. A small classical minimum distance implies a small set of linearly dependent columns in \mathbf{H} . When \mathfrak{r} matches this set, (7) lacks a unique solution, causing BP to stop earlier. Thus, this set leads to a small stopping number.

Increasing check-matrix density may prevent small stopping sets, but sparsity is crucial for low-complexity system implementations. We seek a decoder with strong convergence that is not adversely affected by small stopping sets, rather than increasing check-matrix density. Additionally, we aim to resolve small stopping sets with linear runtime, to prevent quantum information degradation while waiting for the decoder. Efficient algorithms with strong convergence, as proposed in this paper, are essential.

Appendix D: Symmetry of degenerate errors

Strong convergence of GD Flip-BP₂ depends on the code construction, particularly the symmetry of degenerate solutions in the constructed code. This topic is discussed in [55], and we provide more insights here.

Example 4. Consider the binary matrix \mathbf{H} (C1) and $\mathfrak{r} = \{4\}$ as in Example 2. Specifically, we have $[\mathbf{H}_\mathfrak{r}^X | \mathbf{H}_\mathfrak{r}^Z] = \begin{bmatrix} 0 & | & 0 \\ 1 & | & 1 \end{bmatrix}$. The syndrome is the column combination of this matrix and can be either $\mathbf{s}^T = \begin{bmatrix} 0 \\ 0 \end{bmatrix}$ or $\mathbf{s}^T = \begin{bmatrix} 0 \\ 1 \end{bmatrix}$. We are to resolve a feasible solution for $[\mathbf{H}_\mathfrak{r}^Z | \mathbf{H}_\mathfrak{r}^X](\mathbf{E}_\mathfrak{r}^X | \mathbf{E}_\mathfrak{r}^Z)^T = \mathbf{s}^T$ in (7). The feasible solutions $(\mathbf{E}_\mathfrak{r}^X | \mathbf{E}_\mathfrak{r}^Z)$, with $\mathfrak{r} = \{4\}$, are symmetric as follows:

- If $\mathbf{s}^T = \begin{bmatrix} 0 \\ 0 \end{bmatrix}$, we have $(\mathbf{E}_4^X | \mathbf{E}_4^Z) = (0|0)$ or $(1|1)$.
- If $\mathbf{s}^T = \begin{bmatrix} 0 \\ 1 \end{bmatrix}$, we have $(\mathbf{E}_4^X | \mathbf{E}_4^Z) = (1|0)$ or $(0|1)$.

In each syndrome case, we can set any bit arbitrarily to 0 or 1, and then resolve the other bit. Given any \mathbf{s} , the solution is not unique so a bit-flipping BP stops. The GD step in Algorithm 1 will simply set the first bit of $(\mathbf{E}_4^X | \mathbf{E}_4^Z)$ to 1. Then in a subsequent iteration:

- If $\mathbf{s}^T = \begin{bmatrix} 0 \\ 0 \end{bmatrix}$, we obtain $(\mathbf{E}_4^X | \mathbf{E}_4^Z) = (1|1)$.
- If $\mathbf{s}^T = \begin{bmatrix} 0 \\ 1 \end{bmatrix}$, we obtain $(\mathbf{E}_4^X | \mathbf{E}_4^Z) = (1|0)$.

With our proposed GD, the decoder converges in either case.

Example 5. Consider the binary matrix \mathbf{H} (C1) and we take two erasures $\mathfrak{r} = \{2, 4\}$ with syndrome $\mathbf{s} = (010)$ as in Example 1. Restricted to $\mathfrak{r} = \{2, 4\}$, i.e., $\mathfrak{r}_2 = \{2, 4, 6, 8\}$, we have $\mathbf{H}_{\mathfrak{r}_2} = [\mathbf{H}_{\mathfrak{r}_2}^X | \mathbf{H}_{\mathfrak{r}_2}^Z] = \begin{bmatrix} 0 & 0 & | & 0 & 0 \\ 1 & 1 & | & 1 & 1 \\ 0 & 1 & | & 0 & 1 \end{bmatrix}$. To decode, the procedure of Algorithm 1 is shown in Fig. 13, facilitating the understand of the GD Flip-BP₂ algorithm. The decoder converges and outputs IXIY. Another solution, with symmetry at qubit 2, is IZIIY. That is, we can resolve bits 2 and 6 to be either (1|0) or (0|1), and initially, any bit can be resolved arbitrarily to 0 or 1. Similarly, with the symmetry at qubit 4, two additional solutions are IXII and IZII. The four errors are consistent with the four errors in (10).

Due to degeneracy, feasible solutions in Examples 4 and 5 show this **symmetry**: at each erased bit coordinate (within

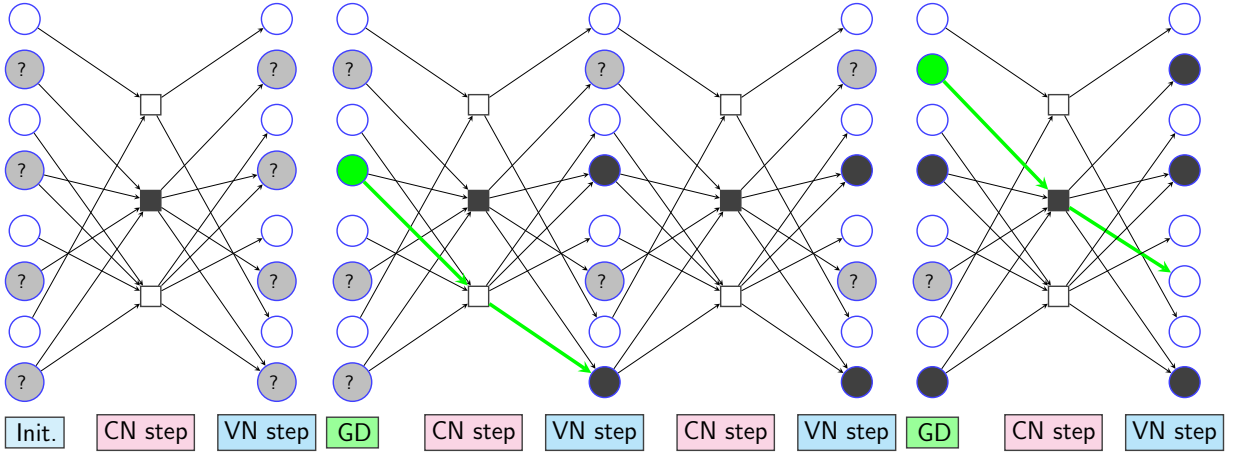


FIG. 13: (coloured online) The decoding process of GD Flip-BP₂ using the binary \mathbf{H} in Example 1 with syndrome $\mathbf{s} = (010)$ and erasures $\mathfrak{r} = \{2, 4\}$, i.e., $\mathfrak{r}_2 = \{2, 4, 6, 8\}$. In the Initialization (Init.), bits 1,3,5,7 are set to 0 (white colour), and bits 2,4,6,8 are set to unknown (with question mark (?)). We present Algorithm 1 as an iterative procedure with check-node and variable-node (CN and VN) computation steps. The 1st iteration has no effective update, so performs GD to set bit 4 to 1 (green colour). This information (green colour) is propagated to correct bit 8 in the 2nd iteration. (Bits with value 1 are with black colour.) The 3rd iteration has no effective update, so performs GD to set bit 2 to 1. This information is propagated to correct bit 6 in the 4th iteration, which resolves all bits. The decoder output is $(0101|0001)$. This is $IXIY$ in Pauli notation, which is an erasure- and syndrome-matched solution.

a small stopping set), both bit values 0 and 1 lead to feasible solutions. A QLDPC matrix typically contains many short cycles and small stopping sets, as discussed earlier. These short cycles lead to overlapping columns in small stopping sets, as shown in previous examples. When erasures cover such small stopping sets, degenerate errors often exhibit the mentioned symmetry property. In this case, GD Flip-BP₂ (Algorithm 1) is likely to resolve the small stopping sets to support successful decoding.

Appendix E: More information about BP

1. Justification of the BP update rules

We justify if Algorithm 2 performs approximation to update $\Lambda_j = \ln \frac{\Pr(\mathbf{E}_j=0)}{\Pr(\mathbf{E}_j=1)}$ to $\Gamma_j = \ln \frac{\Pr(\mathbf{E}_j=0 \mid \text{syndrome is } \mathbf{s})}{\Pr(\mathbf{E}_j=1 \mid \text{syndrome is } \mathbf{s})}$ for the first iteration. We verify this with $\alpha = 1$.

First, by Bayes rule, we write

$$\Gamma_j = \ln \frac{\Pr(\mathbf{E}_j = 0, \text{ syndrome is } \mathbf{s})}{\Pr(\mathbf{E}_j = 1, \text{ syndrome is } \mathbf{s})}. \quad (\text{E1})$$

Assume that the function $\text{soft}(\cdot)$ in (15) is applied on the LLR messages (except the initial Λ_j); this simplifies the derivations below while maintaining good approximation.

We conduct some derivations similar to [77] but focus on binary BP. Denote the row i of \mathbf{H} by \mathbf{H}_i . Then $\mathbf{H}_i|_{\mathcal{N}(i)}$ is the vector of non-zero entries of \mathbf{H}_i . For a vector $\mathbf{v} \in \{0, 1\}^{2^n}$, after measurement, the i -th syndrome bit s_i satisfies $\langle \mathbf{v}, \mathbf{H}_i \rangle = s_i$, or $\langle \mathbf{v}|_{\mathcal{N}(i)}, \mathbf{H}_i|_{\mathcal{N}(i)} \rangle = s_i$. By fixing a bit $v_j = b \in \{0, 1\}$ for some $j \in \mathcal{N}(i)$, we have

$$\langle \mathbf{v}|_{\mathcal{N}(i) \setminus \{j\}}, \mathbf{H}_i|_{\mathcal{N}(i) \setminus \{j\}} \rangle = b + s_i. \quad (\text{E2})$$

We separate s_i and independently write an equation:

$$\langle \mathbf{v}|_{\mathcal{N}(i) \setminus \{j\}}, \mathbf{H}_i|_{\mathcal{N}(i) \setminus \{j\}} \rangle = b. \quad (\text{E3})$$

We compute, for $b \in \{0, 1\}$:

$$\begin{aligned} \Pr(\mathbf{E}_j = b, \text{ syndrome is } \mathbf{s}) &= \sum_{\substack{\mathbf{v} \in \{0,1\}^{2^n}: v_j=b, \\ \langle \mathbf{v}, \mathbf{H}_i \rangle = s_i \forall i}} \Pr(\mathbf{E} = \mathbf{v}) \\ &= \sum_{\substack{\mathbf{v} \in \{0,1\}^{2^n}: v_j=b, \\ \langle \mathbf{v}|_{\mathcal{N}(i)}, \mathbf{H}_i|_{\mathcal{N}(i)} \rangle = s_i \forall i}} \left(\prod_{j'=1}^{2^n} \Pr(\mathbf{E}_{j'} = v_{j'}) \right) \\ &\propto P(\mathbf{E}_j = b) \prod_{i \in \mathcal{M}(j)} \left(\sum_{\substack{\mathbf{v}|_{\mathcal{N}(i) \setminus \{j\}}: \\ \text{satisfy (E2)}}} \Pr(\mathbf{E}|_{\mathcal{N}(i) \setminus \{j\}} = \mathbf{v}|_{\mathcal{N}(i) \setminus \{j\}}) \right), \end{aligned}$$

where $\Pr(\mathbf{E}|_{\mathcal{N}(i) \setminus \{j\}} = \mathbf{v}|_{\mathcal{N}(i) \setminus \{j\}}) = \prod_{j' \in \mathcal{N}(i) \setminus \{j\}} \Pr(\mathbf{E}_{j'} = v_{j'})$ and the approximated proportion (\propto) improves as the Tanner graph contains fewer short cycles. By substituting these results back to (E1), we obtain

$$\begin{aligned} \Gamma_j &= \Lambda_j + \sum_{i \in \mathcal{M}(j)} \ln \frac{\sum_{\substack{\mathbf{v}|_{\mathcal{N}(i) \setminus \{j\}}: \\ \text{satisfy (E2) with } b=0}} \left(\prod_{j' \in \mathcal{N}(i) \setminus \{j\}} \Pr(\mathbf{E}_{j'} = v_{j'}) \right)}{\sum_{\substack{\mathbf{v}|_{\mathcal{N}(i) \setminus \{j\}}: \\ \text{satisfy (E2) with } b=1}} \left(\prod_{j' \in \mathcal{N}(i) \setminus \{j\}} \Pr(\mathbf{E}_{j'} = v_{j'}) \right)} \\ &= \Lambda_j + \sum_{i \in \mathcal{M}(j)} (-1)^{s_i} \ln \frac{\sum_{\substack{\mathbf{v}|_{\mathcal{N}(i) \setminus \{j\}}: \\ \text{satisfy (E3)}}} \left(\prod_{j' \in \mathcal{N}(i) \setminus \{j\}} \Pr(\mathbf{E}_{j'} = v_{j'}) \right)}{\sum_{\substack{\mathbf{v}|_{\mathcal{N}(i) \setminus \{j\}}: \\ \text{satisfy (E3)}}} \left(\prod_{j' \in \mathcal{N}(i) \setminus \{j\}} \Pr(\mathbf{E}_{j'} = v_{j'}) \right)}. \end{aligned} \quad (\text{E4})$$

Algorithm 2, with $\alpha = 1$, resembles this computation by

$$\Gamma_j = \Lambda_j + \sum_{i \in \mathcal{M}(j)} (-1)^{s_i} 2 \tanh^{-1} \left(\prod_{j' \in \mathcal{N}(i) \setminus \{j\}} \tanh \frac{\Gamma_{j'-i}}{2} \right), \quad (\text{E5})$$

where $\Gamma_{j \rightarrow i} = \Lambda_j$ for the first iteration.

Showing that (E5) resembles (E4) requires induction, which is straightforward, e.g., see [77, Appendix A].

2. Fixed inhibition inspired by Hopfield nets

For computing $\Gamma_{j \rightarrow i}$ (12), the message $\Delta_{i \rightarrow j}$ is scaled by $1/\alpha$ in the classical approach. The classical approach assumes that the Tanner graph is without short cycles and tends to resemble a tree—each variable node like a root of the tree and all beliefs from other nodes are properly computed/passed without unwanted cycling information to the root [71, 72]. With this assumption, computing $\Gamma_{j \rightarrow i}$ using the classical approach prevents the cycling of unwanted information. Specifically, in the classical approach,

$$\Gamma_{j \rightarrow i}^{(\text{class})} = \Lambda_j + \left(\frac{1}{\alpha} \sum_{i' \in \mathcal{M}(j)} \Delta_{i' \rightarrow j} \right) - \frac{1}{\alpha} \Delta_{i \rightarrow j} \quad (\text{E6})$$

$$= \Lambda_j + \left(\frac{1}{\alpha} \sum_{\substack{i' \in \mathcal{M}(j) \\ i' \neq i}} \Delta_{i' \rightarrow j} \right). \quad (\text{E7})$$

In the quantum case, a QLDPC matrix induces a Tanner graph with many short cycles, causing this computation to inevitably loop unwanted cycling information.

Fixed inhibition improves the accuracy of Hopfield nets [58–60]. This inspires us to compute

$$\Gamma_{j \rightarrow i} = \Lambda_j + \left(\frac{1}{\alpha} \sum_{i' \in \mathcal{M}(j)} \Delta_{i' \rightarrow j} \right) - \Delta_{i \rightarrow j} \quad (\text{E8})$$

$$= \Lambda_j + \left(\frac{1}{\alpha} \sum_{\substack{i' \in \mathcal{M}(j) \\ i' \neq i}} \Delta_{i' \rightarrow j} \right) + \left(\frac{1}{\alpha} - 1 \right) \Delta_{i \rightarrow j}. \quad (\text{E9})$$

This offers two advantages for decoding stabilizer codes. First, since the Tanner graph contains many short cycles, $\alpha > 1$ is necessary to suppress incorrect information cycling in the algorithm, especially for small-weight errors. In this case, the term $\frac{1}{\alpha} - 1 < 0$ provides extra resistance to such cycled incorrect information. Second, we may also need $\alpha < 1$ to explore multiple degenerate solutions for improved convergence, particularly when the error has a large weight and many degenerate errors share equally likely weights. In this case, the term $\frac{1}{\alpha} - 1 > 0$ enhances local convergence for highly-degenerate codes.

3. Estimating the α value from physical error rate p

We can estimate the value (or at least the trend) of α from the physical error rate. We show this for two scenarios.

First, we estimate the trend of α value solely using the physical error rate p . Without specifying the erasure information \mathfrak{r} , the length $2n$ bit error vector tends to $2n(1-p) + 2np(1/2) = 2n(1 - \frac{p}{2})$ zeros and $2np(1/2) = 2n(\frac{p}{2})$ ones. This is like a binary symmetric channel (BSC) with error rate $p/2$. The corresponding initial LLR is $\Lambda_j = \ln \frac{1-(p/2)}{p/2}$. Assuming equality in (27) and $\Gamma_{j \rightarrow i} = \Gamma_j = \ln \frac{1-(p/2)}{p/2}$, all other variables in (27) are computable and we obtain a proportional trend of α . We plot this in Fig. 14 for different binary row-weight $w_2 = |\mathcal{N}(i)|$ in (27). As shown, α decreases locally linearly with $\log(p)$. If p does not vary significantly, we can model the value of α as a function that decreases linearly in p .

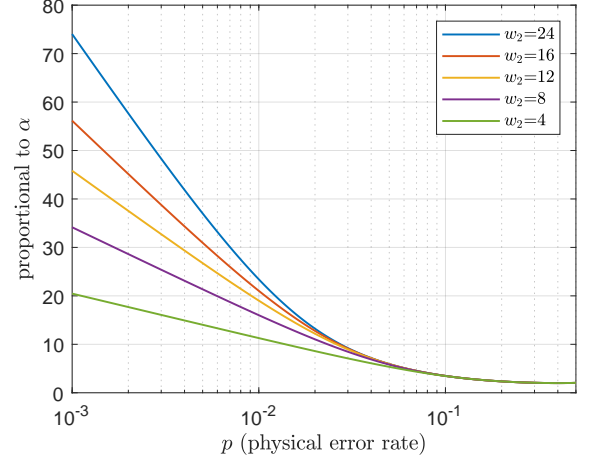


FIG. 14: Estimating α for various physical error rate p at different row-weight w_2 in a binary check matrix.

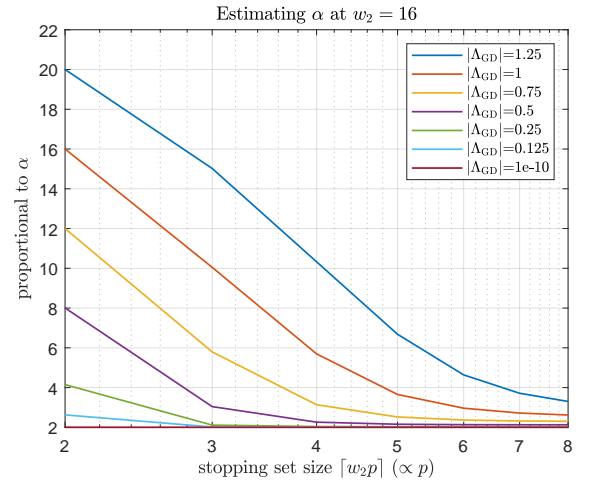


FIG. 15: Estimating α for various $|\Lambda_{\text{GD}}|$ values and stopping set sizes (assumed $\propto p$) at binary row-weight $w_2 = 16$.

Next, we estimate the trend of α value when encountering a stopping set. In this case, other variables outside the stopping set are all determined but cannot help the update in the stopping set. The initial LLRs Λ_j have zero value in the stopping set. To activate updates, here, we reinitialize these Λ_j to have some positive value controlled by a parameter $|\Lambda_{\text{GD}}| > 0$. This will update Γ_j in the stopping set in the next iteration. The value of Γ_j depends on the stopping set size, assumed as $\lceil w_2 p \rceil$. The value of Γ_j also depends on the variable-node degree, assumed as $w_2/2$. (Variable-node degree does not affect the estimation figure but only the scale.) Assuming equality in (27) and using updated $\Gamma_{j \rightarrow i} = \Gamma_j$, we obtain a proportional trend of α . We plot this in Fig. 15 at different stopping set size $\lceil w_2 p \rceil$, assuming a binary row-weight $w_2 = 16$. Different GD values $|\Lambda_{\text{GD}}|$ are tested. Figure 15 suggests that a small $|\Lambda_{\text{GD}}| = 0.25$ is sufficient to trigger effective updates in small stopping sets. Within five iterations ($T_{\text{GD}} = 5$), the value of $|\Gamma_j|$ would ac-

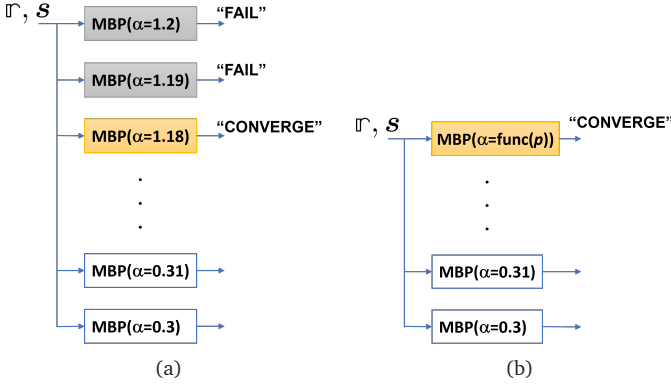


FIG. 16: (a) AMBP with $\alpha_1, \alpha_2, \dots, \alpha_t$ set to 1.2, 1.19, \dots , 0.3 as in (31). (b) The same as (a) but $\alpha_1 = \text{func}(p)$ like (32). Each MBP is efficient, but on “FAIL,” it consumes T_{\max} iterations in (a). In (b), AMBP achieves the efficiency of a successful MBP by choosing a proper α_1 value.

accumulate to be at least 1.25. With this LLR range (0.25 to 1.25), gradients are observed in different stopping set sizes, as shown in Figure 15. Additionally, α again decreases approximately linearly with p locally. We repeat this using different row-weights w_2 , which yield similar results, though the curve slopes differ from Fig. 15.

Choosing α as a locally linear function $\alpha = \text{func}(p)$ accelerates decoding, particularly for AMBP. Figure 16 illustrates how improvement is achieved. We test this in Sec. IV E.

Appendix F: Threshold effect of eBDD

We present an upper bound of (29) that exponentially decreases in n , highlighting the threshold effect of eBDD.

To bound (29), define the typical BDD error probability $P_{\text{BDD}}(n, t', p') := \sum_{j=t'+1}^n \binom{n}{j} (p')^j (1-p')^{n-j}$. Given a fixed ratio $\frac{t'}{n}$ and a small $\varepsilon > 0$, the probability $P_{\text{BDD}}(n, t', p')$ as a function of p' exhibits a sharp decline at $p' = \frac{t'}{n} - \varepsilon$, with exponential decay in n , by a bound from Hoeffding’s inequality (with the condition $t' \geq np'$) [99]:

$$P_{\text{BDD}}(n, t', p') \Big|_{p' = \frac{t'}{n} - \varepsilon} \leq \exp(-2n(\frac{t'}{n} - p')^2) = \exp(-2n\varepsilon^2).$$

An approximate sharper bound, using the Chernoff bound [100] and Kullback–Leibler (KL) divergence (D_{KL}), is:

$$P_{\text{BDD}}(n, t', p') \Big|_{p' = \frac{t'}{n} - \varepsilon} \leq \exp(-2n D_{\text{KL}}(\frac{t'}{n} \parallel p')) \approx \exp(-4n\varepsilon),$$

where $D_{\text{KL}}(p \parallel q) = p \log \frac{p}{q} + (1-p) \log \frac{1-p}{1-q}$ for $p, q \in (0, 1)$ and $D_{\text{KL}}(\frac{t'}{n} \parallel \frac{t'}{n} - \varepsilon) = 2\varepsilon + O(\varepsilon^2)$ by Taylor expansion.

Since $P_{\text{eBDD}}(n, t, p) = P_{\text{BDD}}(n, t', p')$ with $t' = \lceil \frac{3}{4}t \rceil$ and $p' = \frac{3}{4}p$, the function $P_{\text{eBDD}}(n, t, p)$ decays exponentially in n at $p = \frac{t}{n} - \frac{4}{3}\varepsilon$ for a fixed ratio $\frac{t}{n}$ and small $\varepsilon > 0$.

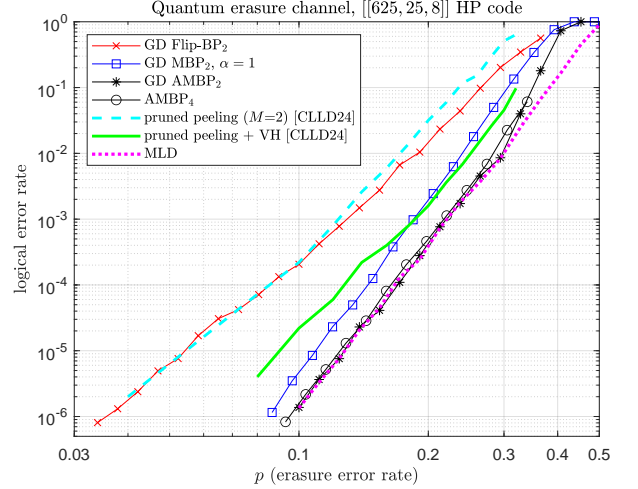


FIG. 17: Comparison of decoders on the $[[625, 25, 8]]$ HP code. The BP and MLD curves are from this paper, and the other two curves from [36] are labelled [CLLD24]. (Only half of the block of the (CSS) code is considered in [36], so we map their decoding failure rate f as $1 - (1-f)^2$ as the logical error rate.) AMBP-type decoders achieve accuracy the same as MLD on this code.

TABLE III: Statistics for the $[[625, 25, 8]]$ HP code. Each data point reflects 100 logical errors (some points here are not shown in Fig. 17). A decoder approaches MLD when its logical error and false convergence rates are similar (Lemma 5, Corollary 6).

	$p=0.107$	$p=0.191$	$p=0.294$
AMBP ₄ logi. error rate	2.55×10^{-6}	0.000289	0.0186
AMBP ₄ false conv. rate	2.45×10^{-6}	0.000251	0.0112
GD AMBP ₂ logi. error rate	2.53×10^{-6}	0.000279	0.00857
GD AMBP ₂ false conv. rate	2.53×10^{-6}	0.000279	0.00840
MLD logi. error rate	2.80×10^{-6}	0.000246	0.00837
MLD false conv. rate	2.80×10^{-6}	0.000246	0.00837

Appendix G: More simulation results

We first compare our decoders with pruned peeling + VH in [36] and BP decoders in [39]. Then we present more simulations for bicycle, LP, and 2D topological codes.

1. HP and GHP codes

Firstly, we consider the HP codes [50]. A $[[625, 25, 8]]$ HP code is studied for erasures using pruned peeling + VH in [36]. We compare it with our decoders. The results are shown in Fig. 17. First, GD Flip-BP₂ performs comparably to the pruned peeling decoder, despite employing a simple GD approach. In contrast, the pruned peeling decoder, with $M = 2$ in Fig. 17, searches through $\binom{m}{2}$ stabilizers to flip bits when escaping from a stopping set, where m is the number of rows in the check matrix. Second, GD MBP₂ with $\alpha = 1$ performs better than the pruned peeling + VH decoder. Finally, for AMBP-type decoders, we select α^* from 1.2, 1.19, \dots , 0.3. Both AMBP₄ and GD AMBP₂ achieve ac-

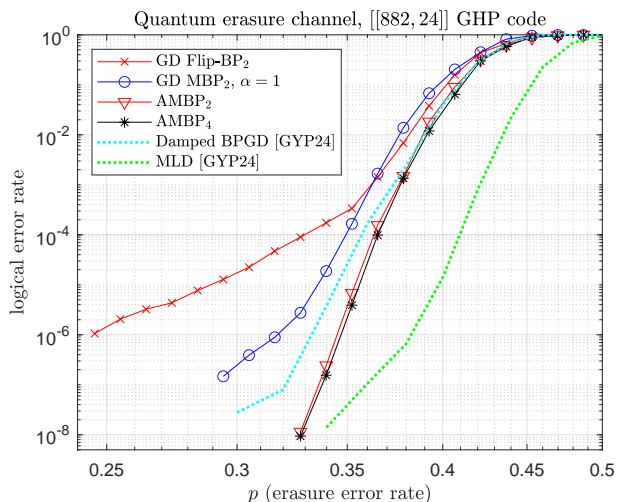


FIG. 18: Comparison of decoders on the $[[882, 24]]$ GHP code.

Curves labelled [GYP24] are from [39, 40], with half-block decoding failure rate converted to logical error rate, as in Fig. 17.

The MLD accuracy is achieved with complexity $O(n^3)$

(unconstrained cluster sizes) [40]. For linear-time decoders, AMBP outperforms Damped BPGD [39] at low logical error rates.

curacy comparable to MLD.

At $p = 0.1$, AMBP₄ or GD AMBP₂ requires an average of 1.8 iterations. GD Flip-BP₂ requires about 1.7 iterations on average at $p = 0.1$, though its decoding accuracy is lower. Similar low average iterations, approximately $O(\log \log n)$, are observed for other codes at low logical error rates.

Here, we implement MLD using Gaussian elimination on (7). We observe that our MLD accuracy is better than the Gaussian decoder in [36]. One possible explanation is that the authors treat the Gaussian decoder as a classical decoding strategy, stating that: it succeeds if $\hat{e} = e$. If so, then this does not account for degeneracy (Def. 4). In our implementations, we always account for degeneracy (Def. 5). Furthermore, in Fig. 17, we verify whether our decoders achieve MLD accuracy using Lemma 5 and Corollary 6. Table III presents the logical error and false convergence rates for several decoders. A decoder closely achieves MLD if and only if the two rates are approximately equal. Table III confirms this expectation.

Secondly, we decoder an $[[882, 24, d]]$ GHP code from [56], where $18 \leq d \leq 24$. The results are shown in Fig. 18. BP enhanced with damping and guided decimation (Damped BPGD) [39] encounters additional decoder error floor, not reaching MLD accuracy at low error rates. Decoding via peeling + cluster decomposition [40] requires unconstrained cluster sizes, resulting in $O(n^3)$ complexity like the Gaussian decoder to achieve MLD. For our decoders, AMBP-type decoders achieve strong accuracy, significantly outperforming Damped BPGD at low logical error rates. At $p = 0.328$, AMBP₄ achieves similar logical error and false convergence rates of 9.4×10^{-9} and 4.15×10^{-9} , respectively. By Corollary 6, AMBP decoders closely achieve MLD at low error rates.

TABLE IV: Parameters of binary check matrices H (mean column and row weights (j_2, w_2)) and Pauli check matrices H (mean column and row weights (j, w))[†]. These codes have $w = w_2$.

type	rate	n of tested codes	j_2	j	w
bicycle	3/4	946, 1892, and 3786	≈ 4.5	≈ 9	34–38
bicycle	1/2	946, 1892, and 3786	≈ 4.5	≈ 9	18
bicycle	1/4	946, 1892, and 3786	≈ 5	≈ 10	12–14
LP	0.118	1054, 2210, and 4114	3	6	8
LP	0.04	925, 2075, and 4075	3	6	7
toric	$\rightarrow 0$	16, 64, 144, 324	2	4	4
XZZX	$\rightarrow 0$	5, 13, 61, 145	2	4	4

[†] BP memory and runtime complexity scale with the number of messages: $2nj_2$ for the binary matrix H and nj for the Pauli matrix H . Notably, codes within the same family have nearly fixed j or j_2 , ensuring linear complexity.

2. Parameters of families of codes with constant rate

In the following, we consider families of codes with constant rate. We first summarize the parameters of tested codes and link them to the memory and runtime complexity. According to our algorithms, it is easy to deduce that BP memory size is proportional to the number of messages: $O(2nj_2)$ for binary BP and $O(nj)$ for quaternary BP, where j_2 and j are the mean column-weights of the binary or quaternary check matrices, respectively. We present the parameters of n , j , j_2 , as well as the stabilizer weight w for each code family, in Table IV. As shown, for each code family, the memory complexity remains linear, $O(n)$, since j_2 and j are nearly fixed for each code family.

For computational complexity, each iteration of BP has a complexity proportional to the number of messages, $O(2nj_2) = O(nj)$ for each code family, which is linear in n for a code family with fixed j . This per-iteration linear runtime is shown in practical measurements [57, Fig. 7]. The overall BP complexity is $O(nj\tau)$, where τ is the average iteration count. Classically, BP achieves good convergence at low decoding block error rates with $\tau = O(\log \log n)$ [68, 71], which is essentially constant time. We observe a similar convergence rate for our BPs on the QLDPC codes (e.g., see Table II). Thus, BP complexity is $O(n \log \log n)$ for each code family as n increases and j remains fixed.

3. Bicycle codes

Bicycle codes offer flexible length and rate, and demonstrate performance close to the quantum Gilbert-Varshamov bound for correcting depolarizing errors [17, 57].

We construct bicycle codes with varying code rates $r = \frac{k}{n}$ and row-weights w using random generator vectors. A key step in this construction is row-deletion, which requires heuristics [17]. Herein, we employ a greedy algorithm that deletes a group of 32 rows at a time, until 64 rows remain to be deleted, one at a time, while maintaining small resultant column-weight variance throughout the process. The bicy-

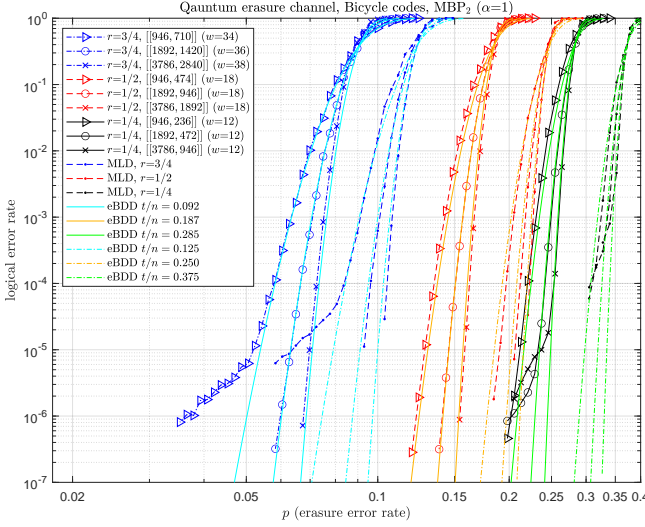


FIG. 19: Accuracy of MBP_2 and MLD on bicycle codes. The error floors arise from the codes, as shown by MLD curves. The decoders (A) MBP_q have accuracy comparable to MBP_2 on these codes. GD Flip- BP_2 shows similar accuracy but has a higher error floor on the $[[1892, 492]]$ code (remaining below 10^{-4} [101]). Increasing the row-weight w can suppress error floors (cf. Fig. 6).

cle construction results in a Pauli check matrix with a mean column-weight $j \approx w(1-r)$. We construct three families of bicycle codes, all with a mean column-weight $j \approx 9$:

- Rate $1/4$, $w = 12$, $j \approx 9$: $n = 946, 1892, 3786$.
- Rate $1/2$, $w = 18$, $j \approx 9$: $n = 946, 1892, 3786$.
- Rate $3/4$, $w \approx 36$, $j \approx 9$: $n = 946, 1892, 3786$ with $w = 34, 36, 38$, respectively.

For these bicycle codes, MBP_2 with $\alpha = 1$ and a parallel schedule (the default message-update order in Algorithm 2) is sufficient for decoding. AMBP or other schedules do not provide further improvement. We present MBP_2 accuracy and compare it to MLD in Fig. 19. With eBDD (29), we estimate the threshold values for BP and MLD at each code rate, as shown in the figure legend. BP achieves thresholds approximately 0.092, 0.187, and 0.285 for rates $3/4$, $1/2$, and $1/4$, respectively. MLD achieves higher thresholds approximately 0.125, 0.25, and 0.375 for rates $3/4$, $1/2$, and $1/4$, respectively. Some codes have error floors. We review the raw data and the BP error floor indicates the MLD error floor (Corollary 6), i.e., the error floors are from the codes.

GD Flip- BP_2 is well-suited for decoding bicycle codes when low decoding complexity is essential. It achieves similar BP accuracy as shown in Fig. 19, except for one code $[[1892, 492]]$, which results in a higher error floor, but still below 10^{-4} . GD Flip- BP_2 accuracy on these bicycle codes is shown in an earlier version of this paper [101, Fig. 9].

The error floor can be suppressed by increasing the row-weight w (which could increase the code distance [17]). For codes with error floors in Fig. 19, we increase w for

TABLE V: Parameters of QC matrices (j , w , m , and girth) of the $[[n, k]]$ LP codes employed in this paper.

Asymptotic rate 0.118:					
j	w	m	girth	$[[n, k]]$	from
3	5	31	8	$[[1054, 140]]$	[18] [†]
3	5	65	8	$[[2210, 276]]$	this paper
3	5	121	10	$[[4114, 500]]$	this paper

[†] The base matrix is from [26].

Asymptotic rate 0.04:					
j	w	m	girth	$[[n, k]]$	from
3	4	37	8	$[[925, 49]]$	this paper
3	4	83	10	$[[2075, 95]]$	this paper
3	4	163	10	$[[4075, 175]]$	this paper

constructions. The decoding results, as shown in the main text (Fig. 6), are free of error floors.

4. LP codes

LP codes generalize the GHP construction to allow flexible lengths and rates [18]. We focus on LP codes derived from classical quasi-cyclic (QC) matrices, based on the method in [18, Example 3].

In this subsection, j, w, m and the girth value represent the parameters of the underlying QC matrix.

A QC matrix [26, 91] is defined by a $j \times w$ base matrix, where each entry represents a circulant matrix with a specific cyclic shift from an $m \times m$ identity matrix. This results in a sparse binary $jm \times wm$ QC matrix, which we use to construct an LP code with parameters $n = m(w^2 + j^2)$ and $k \geq m(w - j)^2$, following the construction method in [18, Example 3]. The asymptotic rate is given by $r = (w - j)^2 / (w^2 + j^2)$. Our constructed QC matrices have parameters listed in Table V. The constructed base matrices are in (G1)–(G6), as follows.

For asymptotic rate 0.118, the base matrices:

$$m = 31; \quad \text{girth } 8; \quad \begin{bmatrix} 1 & 2 & 4 & 8 & 16 \\ 5 & 10 & 20 & 9 & 18 \\ 25 & 19 & 7 & 14 & 28 \end{bmatrix} \text{ (from [26])}. \quad (\text{G1})$$

$$m = 65; \quad \text{girth } 8; \quad \begin{bmatrix} 30 & 32 & 57 & 37 & 23 \\ 19 & 7 & 53 & 64 & 47 \\ 47 & 7 & 63 & 37 & 21 \end{bmatrix}. \quad (\text{G2})$$

$$m = 121; \quad \text{girth } 10; \quad \begin{bmatrix} 55 & 60 & 106 & 118 & 88 \\ 36 & 13 & 95 & 70 & 37 \\ 86 & 13 & 71 & 44 & 31 \end{bmatrix}. \quad (\text{G3})$$

For asymptotic rate 0.04, the base matrices:

$$m = 37; \quad \text{girth } 8; \quad \begin{bmatrix} 17 & 19 & 33 & 21 \\ 11 & 4 & 31 & 0 \\ 27 & 4 & 36 & 21 \end{bmatrix}. \quad (\text{G4})$$

$$m = 83; \quad \text{girth } 10; \quad \begin{bmatrix} 38 & 41 & 73 & 47 \\ 25 & 9 & 65 & 42 \\ 59 & 9 & 81 & 62 \end{bmatrix}. \quad (\text{G5})$$

$$m = 163; \quad \text{girth } 10; \quad \begin{bmatrix} 74 & 80 & 143 & 92 \\ 48 & 18 & 129 & 159 \\ 116 & 17 & 156 & 84 \end{bmatrix}. \quad (\text{G6})$$

In these base matrices, an entry value of 0 indicates an $m \times m$ identity sub-matrix $\mathbf{1}_m$, while a positive value indicates a circulant matrix derived from $\mathbf{1}_m$ with shift amount specified by the value. The cyclic shift can be a row shift

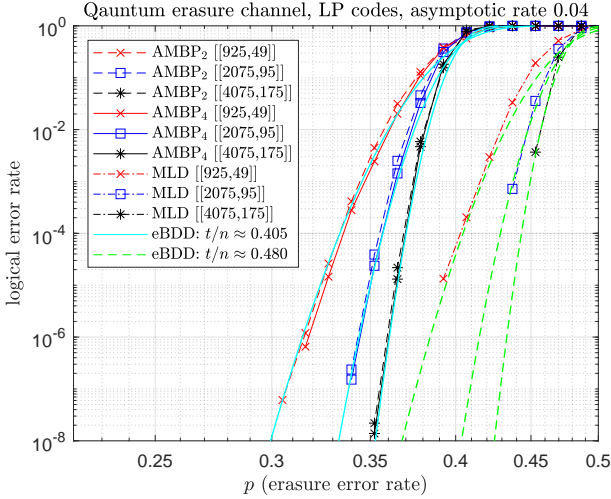


FIG. 20: Accuracy of AMBP and MLD on rate 0.04 LP codes. Our AMBP_q exhibit a threshold of $p_{\text{th}} = 0.405$. MLD curves suggest a higher threshold of $p_{\text{th}} = 0.48$. (For rate 0.118 case, see Fig. 7.)

(rightward) [91] or a column shift (downward) [18]. We adopt the column shift.

The constructed QC matrices are regular, which produces classical codes almost without error floors [68, 71]. We construct regular QC matrices following techniques in [92], conducting multiple random trials to maximize girth and prevent small stopping sets in QC matrices (Remark 7).

After lifted-product, the girth of the resultant quantum code is Unknown. We evaluate code performance through simulations. AMBP-type decoders provide the best BP accuracy for LP codes. The decoding accuracy for rate 0.118 case is presented in the main text (Fig. 7). For rate 0.04 case, it is shown in Fig. 20, where MLD achieves a threshold of 0.48, while AMBP achieves a threshold of 0.405.

Several shorter LP codes are constructed in [102]. We decode these codes for erasures, and observe error floors. We do not observe error floors in our constructed codes. A key distinction lies in the QC matrices: [102] employs a typical QC matrix [91] containing many identity sub-matrices (zero circulant shift), while we construct QC matrices with fully random circulant shifts [26, 92].

Incorporating some $m \times m$ zero matrices in a QC matrix yields an irregular QC matrix, potentially increasing the girth. This adjustment enables BP to exhibit better accuracy, though it requires careful construction to avoid error floors [103]. We construct several irregular LP codes that show potential for achieving higher BP thresholds, as discussed in the earlier version of this paper [101].

5. Topological codes

AMBP_4 provides the best BP accuracy on topological codes. The accuracy of AMBP_4 and MLD on the toric and XZZX is shown in the main text (Fig. 9) to illustrating a threshold of 0.5 for both decoders. We present their accu-

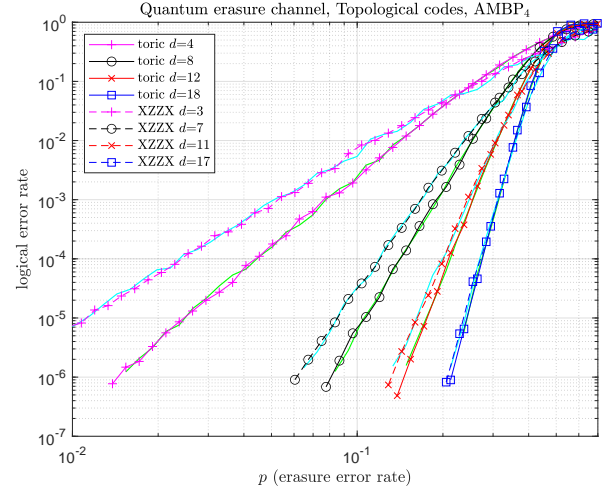


FIG. 21: Accuracy of of AMBP_4 and MLD on the toric and XZZX codes at low error rates. The two decoders have the same accuracy. (MLD curves are green and cyan lines, as in Fig. 9.)

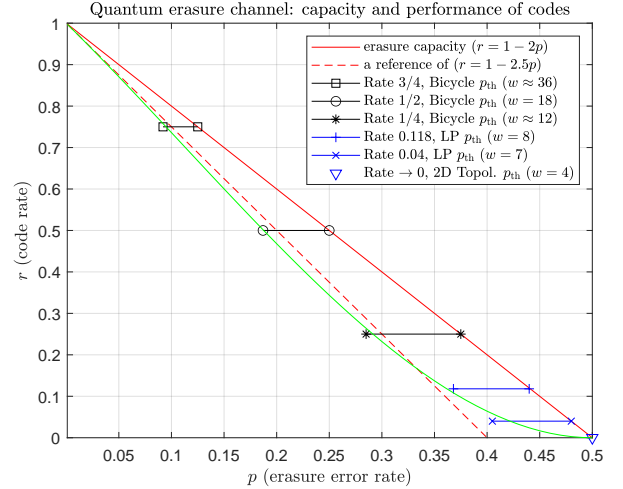


FIG. 22: Replotting Fig. 2 with p on a linear scale. Performance achieved by BP is $r = 1 - 2.5p - 2p^2 + 6p^3$ (green line).

racy on a log scale in Fig. 21, showing that AMBP_4 matches MLD at low error rates.

6. Erasure capacity and code thresholds

Here, we replot Fig. 2 on a linear scale to present the decoder accuracy. The results are shown in Fig. 22. Using MLD, we obtain capacity-achieving performance. Using linear-time BP decoders, we achieve capacity performance with topological codes for rate $r \rightarrow 0$. For $r > 0$, LP and bicycle codes yield performance approximately equal to $r = 1 - 2.5p$. To obtain a more precise estimate by interpolation, the performance achieved by BP is approximately $r = 1 - 2.5p - 2p^2 + 6p^3$.

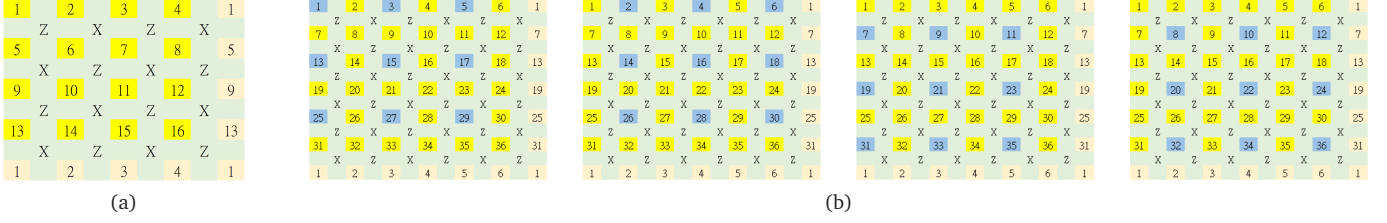


FIG. 23: (a) Lattice representation of the $[[16, 2, 4]]$ toric code. (b) Group partition of the $[[36, 2, 6]]$ toric code using quaternary BP. In (a), a qubit is represented by a yellow box numbered from 1 to $n = 16$. Each orange box on the right and bottom represents the qubit of the same number. An X - or Z -type stabilizer is indicated by a label $W \in \{X, Z\}$ between its neighbouring qubits. In (b), we show the partitioning of a toric code into four groups for BP_4 . Blue colour indicates which variable nodes are in one group. All nodes within each group are processed in parallel. The four groups are processed in serial, and this serial order is randomized in each iteration.

Appendix H: BP schedule and parallelism

When (A)MBP is used, we consider two different schedules. The first is the parallel schedule, with a message updating order as in Algorithm 2.

It is known that a serial schedule may offer the advantage of better convergence [61], especially when decoding highly-degenerate codes [57]. With some pre-simulations, we observe that randomizing the serial order in each iteration helps prevent the decoder from getting trapped in the same stopping set. To maintain parallelism, we propose a *group random schedule* derived from a given (binary or quaternary) Tanner graph, described as follows. A comparable method is presented in [104] and we will discuss it later.

First, **partition rule**: partition the variable nodes into groups; variable nodes that have independent messages within an iteration are assigned to the same group. Variable nodes j_1 and j_2 belong to the same group if their neighbouring check node sets have an empty intersection, $\mathcal{M}(j_1) \cap \mathcal{M}(j_2) = \emptyset$. Next, **group-based random order**: during decoding, variable nodes within a group are processed in parallel and groups are processed in serial; the serial order is further randomized in each iteration.

This is better illustrated by using topological codes and quaternary BP. We show the 4×4 toric code in Fig. 23(a), explaining the code structure. Then we show the 6×6 toric code in Fig. 23(b), illustrating the partition of groups. The 36 variable nodes are partitioned into 4 groups using the above partition rule.

Next, we also use the toric codes and quaternary BP to explain the group random schedule. For a toric lattice of with n data qubits, the group size is $n/4$ and there are four groups. If we have $n/4$ cores, the messages of all nodes within each group are processed in parallel. However, the four groups are processed in serial, and this serial order is randomized in each iteration. In software simulations, this is modelled by a random serial order, where one group is followed by another. The internal order of the nodes within a group does not affect the simulation of this schedule.

The group random schedule offers the advantage of high

parallelism while maintaining strong convergence, and it is applicable to general QLDPC codes.

We decompose variable nodes into groups, and test our method for various QLDPC codes in this paper. In [104], check nodes are decomposed into layers (groups), and the method is validated on (G)HP codes. Our method is a partially parallel version of the random serial schedule along variable nodes, while [104] applies it along check nodes. We find that scheduling along variable nodes tends to better exploits degeneracy, especially for topological codes. This warrants further investigation.

Appendix I: Numerical stability and message softization

When a soft-valued BP algorithm, such as (A)MBP is employed, message values must be constrained to ensure numerical stability. Based on our experience, the initial distributions do not require adjustment; the most effective approach is to constrain the variable-to-check messages.

To maintain numerical stability for LLR, the function $\text{soft}(\cdot)$ in (15) imposes LLR_MAX and LLR_MIN with values 35 and 10^{-10} , respectively, as calculated in Box 1. The calculation considers a check matrix with row-weight 30 and assumes a worst-case scenario where all incoming messages to a check node are at extreme values, a situation that is rare. Even if row-weight > 30 and underflow (or overflow) occurs, subsequent iterations restore stability by reapplying the constraint on variable-to-check messages again.

An LLR algorithm can be converted into a linear-domain algorithm with scalar messages representing the probability difference between commute and anti-commute. Compare Algorithms 1 and 3 in [57, arXiv version] for LLR MBP_4 and linear MBP_4 . A similar conversion applies to MBP_2 . Box 2 shows how constraints are applied to the linear difference messages to equivalently implement the function (15).

Note that non-zero message values arise after applying our constraints, ensuring numerical stability for (19) and enabling BP updates within stopping sets.

```

/-- prevent extreme LLR values
#define LLR_MAX (38) // IEEE754 double 1.0-tanh(38.1/2) = 1.110223024625157e-16 , but 1.0-tanh(38.2/2) = 0 (NG)
//define LLR_MAX (36) // very extreme since if >36, sometimes makes LLR decoder messages Dm[m]=0
#define LLR_MAX (35) // IEEE754 double tanh(35.9/2) = 0.9999999999999999 , protected from tanh(36/2) = 1 (OK)
#define prevent_llr_ov(llr) { \
  if(llr > LLR_MAX) { llr = LLR_MAX; } \
  else if(llr < -LLR_MAX) { llr = -LLR_MAX; } \
}
/-- prevent LLR to be too close to zero
#define LLR_MIN (1.0e-10) // support up to row weight 30, since tanh(1e-10/2)^30 = 9.313225746154796e-310 ~= |DBL_MIN|
#define prevent_llr_0(llr) { \
  if(llr < LLR_MIN) { \
    if(llr >= 0) { llr = LLR_MIN; } \
    else if(llr > -LLR_MIN) { llr = -LLR_MIN; } \
  } \
}
/-- restrict LLR in reasonable range
#define restrict_llr(llr) { \
  if(llr > LLR_MAX) { llr = LLR_MAX; } \
  else if(llr < LLR_MIN) { \
    if(llr >= 0) { llr = LLR_MIN; } \
    else if(llr > -LLR_MIN) { llr = -LLR_MIN; } \
    else if(llr < -LLR_MAX) { llr = -LLR_MAX; } \
  } \
}

```

Box 1

```

/-- prevent extreme linear values
#define dlt (1e-11) // note, log10((2e-11)^30) = -320.97 (still > DBL_MIN 5e-324 even if row_wt=30);
#define restrict_p2(p) \
{ \
  if(p[0] < dlt_b) { \
    p[0] = dlt_b; p[1] = 1.0 - dlt_b; \
  } \
  else if(p[0] > 1.0 - dlt_b) { \
    p[0] = 1.0 - dlt_b; p[1] = dlt_b; \
  } \
  else if(0.5-dlt_b < p[0] && p[0] < 0.5+dlt_b) { \
    if(p[0] < 0.5) { p[0] = 0.5-dlt_b; p[1] = 0.5+dlt_b; } \
    else { p[0] = 0.5+dlt_b; p[1] = 0.5-dlt_b; } \
  } \
  else { p[1] = 1.0 - p[0]; } \
}

```

Box 2